ENVIRONMENTAL AND BIOLOGICAL CONTROLS ON CARBON DIOXIDE AND METHANE EXCHANGE IN A RESTORED FRESHWATER MINERAL-SOIL WETLAND AT FRANK LAKE, ALBERTA

WEERAHANNEDIGE OSHINI KAUSHALYA FERNANDO
Bachelor of Science, University of Sri Jayewardenepura, Sri Lanka, 2019

A thesis submitted
in partial fulfilment of the requirements for the degree of

MASTER OF SCIENCE

in

BIOLOGICAL SCIENCES

Department of Biological Sciences
University of Lethbridge
LETHBRIDGE, ALBERTA, CANADA

ENVIRONMENTAL AND BIOLOGICAL CONTROLS ON CARBON DIOXIDE AND METHANE EXCHANGE IN A RESTORED FRESHWATER MINERAL-SOIL WETLAND AT FRANK LAKE, ALBERTA

WEERAHANNEDIGE OSHINI KAUSHALYA FERNANDO

Date of Defense: December 4, 2023

Dr. L. B. Flanagan Thesis Supervisor	Professor	Ph.D.
Dr. S. B. Rood Thesis Examination Committee Member	Professor Emeritus	Ph.D.
Dr. M. J. Bogard Thesis Examination Committee Member	Assistant Professor	Ph.D.
Dr. L. Chasmer Thesis Examination Committee Member	Associate Professor	Ph.D.
Dr. Dmytro Yevtushenko Chair, Thesis Examination Committee	Associate Professor	Ph.D.

ABSTRACT

Prairie pothole wetlands have been shown to be strong sinks for carbon dioxide (CO_2); however, it is likely that these ecosystems are also strong emitters of methane (CH_4), reducing their overall carbon (C) sequestration potential. This study presents growing season (May-September 2022) eddy covariance flux measurements of CO_2 and CH_4 at a prairie pothole wetland near High River, Alberta with extensive bulrush (*Schoenoplectus acutus*) vegetation. The study was conducted during a time-period that was warmer and had precipitation inputs that were altered from the long-term average pattern. Despite the warmer and relatively dry weather in 2022, the wetland was still an important sink for atmospheric CO_2 during the study period with a net uptake of 49 g C m^{-2} resulting from 623 g C m^{-2} of photosynthesis and 575 g C m^{-2} of respiration. Methane flux expressed in CO_2-equivalents (6 g C m^{-2} $season^{-1}$) offset only ~12% of carbon sequestration based on CO_2 only. This suggests that the valuable ecosystem service of C sequestration can still occur in a prairie pothole wetland even in warm and dry weather conditions.

ACKNOWLEDGEMENTS

I would like to extend my deepest gratitude to my thesis supervisor, Dr. Lawrence B. Flanagan, for the immense guidance, and encouragement he provided throughout my study. I extend my heartfelt gratitude to the members of my thesis committee, Prof. Stewart Rood, Dr. Matthew Bogard, and Dr. Laura Chasmer for providing their expertise and insightful contributions in shaping the outcome of my research.

I also wish to thank Dr. M. J. Bogard for letting me attend his weekly lab meetings. I appreciate Kaydunn Henry, Dani Nadeau and Henry Bain for their assistance given during fieldwork. I gladly acknowledge the advice and assistance provided by Oscar Zimmerman and Kristian Smits, the senior graduate students in my lab group.

To my loving parents and two sisters, I am deeply grateful for the support they have provided throughout my academic journey. I am truly grateful to my devoted and supportive best friend Nadia Hand, for consistently standing by my side. I would like to express my heartfelt appreciation to my beloved husband, Malindu. His belief in my abilities, unwavering support, countless sacrifices, and love have been the pillars of strength that have carried me through the ups and downs of my program.

This study was made possible by research grant funds to L. B. Flanagan from the Natural Sciences and Engineering Research Council of Canada (NSERC) Alliance Program and Alberta Innovates. I am grateful to the McCain Foundation for offering me the McCain Studentship Award during my studies which allowed me to focus on my research and pursue academic excellence.

TABLE OF CONTENTS

LIST OF TABLES

LIST OF FIGURES

LIST OF ABBREVIATIONS AND SYMBOLS

Carbon dioxide (CO_2)
Normalized difference vegetation index (NDVI)
Methane (CH_4)
Nature-based solution (NBS)
Ducks Unlimited Canada (DUC)
Photosynthetically active photon flux density (PPFD)
Frank Lake Basin 3 East (FLB3E)
Leaf area index (LAI)
Sensible heat flux (H)
Latent heat flux (LE)
Coefficient of determination (r^2)
Eddy covariance (EC)
Gross primary productivity (GPP)
Gross ecosystem productivity (GEP)
Total ecosystem respiration (TER)
Net ecosystem exchange (NEE)
Soil water potential (SWP)
Soil volumetric water content (SVWC)
Prairie pothole region (PPR)

CHAPTER 1: INTRODUCTION

1.1 Background

Given the repercussions of climate change around the world, global warming mitigation is an issue that needs to be addressed immediately (Kayranli *et al.*, 2009). Wetlands are one of the most important ecosystems that help to regulate climate change by sequestering C (Were *et al.*, 2019), which is the process of assimilating CO_2 from the atmosphere (Kayranli *et al.*, 2009). Wetlands typically have high biomass production, high water tables and low decomposition rates, which allow them to retain C in the soil, sediment, and debris (Whitting and Chanton, 2001). Wetland soils are estimated to contain up to one-third of the C that is present in organic soils worldwide (Were *et al.,* 2019), although only making up 5 to 8% of the Earth's land surface (Nahlik and Fennessy, 2016). Wetlands are either ineffectively managed or are being continuously destroyed at an alarming rate despite their values and functions in providing ecological services (Sinthumule, 2021). Degraded wetlands and their lost functions can be regained through wetland restoration (Were *et al.*, 2019) and thus, restoration of wetlands is suggested as an effective and sustainable nature-based solution (NBS). NBS are actions to protect, sustainably manage and restore natural or modified ecosystems, which address societal challenges effectively and adaptively while also providing benefits to human well-being and biodiversity, according to the International Union for Conservation of Nature (IUCN) (Cohen-Shacham *et al.*, 2016).

Wetlands play a crucial role in the global C cycle because they are both C sources and sinks, storing C in soils and vegetation as well as emitting CO_2 and CH_4 into the

atmosphere (Olsson *et al.,* 2015). Even though at a slower rate than photosynthesis, aerobic and anaerobic decomposition of organic matter also occurs in wetlands. Aerobic decomposition is more efficient and forms CO_2 as the principal end-product. In contrast, anaerobic decomposition is significantly slower and produces CH_4 in addition to CO_2 (Olsson *et al.,* 2015), contributing to about 30% of total global CH_4 emissions (Petrescu *et al.,* 2015). Both CO_2 and CH_4 are greenhouse gases (GHGs) that contribute to global warming. Currently, CH_4 stands as the second most important GHG, following CO_2, contributing to approximately 16–25% of the warming observed in the Earth's atmosphere (Rosentreter *et al.,* 2021). Due to the 45-fold higher sustained global warming potential (SGWP) compared to CO_2 over a 100-year span, large CH_4 emissions could cause disproportionately adverse climate impacts (Neubauer and Megonigal, 2015). In wetlands, the CO_2 and CH_4 cycles are complex, involving simultaneous and interacting processes. These processes include microbial CH_4 production and oxidation in the soil, alongside CO_2 absorption through photosynthesis and release through ecosystem respiration (Helfter *et al.*, 2022). Therefore, to determine if a wetland is a source or a sink for GHGs, understanding the balance between CO_2 and CH_4 fluxes is important and studying the factors which drive these fluxes helps us understand the effects of ecosystem processes on future climate patterns (Hemes *et al.,* 2018).

Plants, both vascular and non-vascular (like mosses), absorb CO_2 through leaf pores (stomata) and cell walls respectively. This is important for photosynthesis, where plants utilize sunlight to transform water and CO_2 into carbohydrates for growth. Carbon dioxide is emitted through plant respiration from leaves, barks, and roots. Additionally, microbial decomposition during the consumption of dead plant material

also releases CO_2 (Lafleur, 2009). The difference between CO_2 uptake through gross primary production (GPP) and subsequent loss through autotrophic and heterotrophic respiration, collectively referred to as total ecosystem respiration (TER), represents the net ecosystem exchange of CO_2 (CO_2 NEE) between the ecosystem and the atmosphere (Chapin *et al.,* 2006, Lund *et al.,* 2010). The seasonal variations in CO_2 exchange within marsh ecosystems are closely linked to the growth and senescence of macrophytes, influenced by light and temperature (Strachan *et al.*, 2015). Bonneville *et al.,* (2008) have demonstrated that in temperate and boreal regions, the seasonal pattern in daily CO_2 NEE within a specific wetland, correlates strongly with the progression of the vegetation canopy, commonly indicated by the seasonal fluctuation in leaf area index (LAI).

Following the stepwise breakdown of organic matter under anoxic conditions, methanogenic archaea generate CH_4 in wetland sediments and soils (Segers, 1998). After being produced, CH_4 can either be oxidized by aerobic methanotrophic bacteria or it can move to the water or soil surface and be released into the atmosphere through diffusion, ebullition, or plant-mediated transport (Villa *et al.*, 2020). The diversity in morphological and physiological traits of wetland plants significantly influences the activity of microbes involved in both CH_4 production and consumption, as well as the rate of CH_4 transport to the atmosphere (Bubier & Moore, 1994; Joabsson *et al.*, 1999). Plants also generate carbohydrates during photosynthesis, which can be released as "root exudates" and CO_2 during respiration. These plant products serve as substrates for methanogenesis (Long *et al.*, 2010). Some wetland plants have an internal network of air spaces called aerenchyma, which creates a direct gas-phase connection between the atmosphere and soil environments. This enables quick gas exchange because gases

diffuse 10^4 times more quickly in air than through water (Sorrell and Brix, 2013). The aerenchyma of plant tissue can also help CH_4 created in the soil to bypass the water column, where resident methanotrophs can oxidize it before it reaches the atmosphere (Whalen, 2005). Passive molecular diffusion, following concentration gradients within aerenchyma and convective flow (bulk flow) of air through aerenchyma can supply O_2 to the anoxic rhizosphere, forcing CO_2 and CH_4 out of plant roots into the atmosphere (Brix, 1993) and lead to inhibition of methanogenesis and oxidation of CH_4 (Joabsson and Christensen, 2001). Plants also have the potential to uptake and release water containing dissolved CH_4 (Long *et al.*, 2010). Therefore, plant-mediated transport is a crucial gas transport pathway, in addition to diffusion and ebullition, enhancing CH_4 emissions to the atmosphere (Olsson *et al.*, 2015). Furthermore, environmental factors, such as air and soil temperature fluctuations, water table depth, and substrate availability for methanogens, result in considerable spatial and temporal variations in CH_4 emissions (Petrescu *et al.*, 2015).

In natural wetlands, diverse environmental factors regulate the balance between photosynthetic and respiratory processes, influencing the net C accumulation in biomass and soil, as well as the production, transport, consumption, and release of CH_4. Therefore, these environmental factors have a substantial impact on temporal and spatial variation in CH_4 and CO_2 emissions (Petrescu *et al.,* 2015). Organic matter decomposition in wetland soils is strongly dependent on temperature, and therefore, both CO_2 and CH_4 emissions from decomposition processes tend to increase with increasing soil temperature (Herbst *et al.,* 2011). However, laboratory and field experiments have shown that CH_4 fluxes are more sensitive to temperature change than CO_2 fluxes due to differences in the biochemical kinetics of methanogenesis and

respiration (Chen *et al.,* 2021). The position of the water table determines the extent of the anoxic soil zone, where CH_4 is produced. Additionally, it influences the oxic soil zone, where CH_4 is oxidized (Walter and Heimann, 2000). Therefore, the water table position plays a pivotal role in regulating CH_4 emissions, with increased water tables causing O_2 depletion and fostering methanogenesis in wetland soil (Grunfeld and Brix, 1999). More oxidized conditions favour CH_4 oxidation by aerobic methanotrophic bacteria (Whalen, 2005), as well as aerobic decomposition of organic matter, both processes emitting CO_2. While CO_2 and CH_4 fluxes in wetlands are heavily influenced by wetland hydrology, the impact of fluctuating water tables on these fluxes can be unpredictable (Helfter *et al.*, 2022). For instance, ecosystem respiration shows varied responses to water table changes, increasing or decreasing based on the position of the water table (Gomez-Casanovas *et al.*, 2020). In addition, episodic salinization which can affect some freshwater wetlands, has been shown to disproportionately decrease gross ecosystem productivity (GEP) compared to CH_4 fluxes, leading to an overall increase in wetland GHG emissions during peak salinity (Chamberlain *et al.,* 2018).

Greenhouse gases (GHGs) exhibit varying atmospheric lifetimes and radiative efficiencies, reflecting their ability to absorb and re-radiate infrared radiation. The Global Warming Potential (GWP) is commonly used to compare the relative radiative forcing of gases with diverse characteristics. By converting GHG fluxes to CO_2-equivalents using GWP, ecosystems' net warming or cooling effects on global climate can be directly assessed (Neubauer and Megonigal, 2015). However, GWP is not suitable for ecosystems with sustained GHG fluxes over time. To address this limitation, the Sustained Global Warming Potential (SGWP) was introduced,

specifically considering gas emissions as persistent events (Neubauer and Megonigal, 2015).

Gas exchanges between the surface and atmosphere must be regularly monitored since the ecosystem's C balance might be altered by environmental or meteorological changes (Bonneville *et al.,* 2008). With recent advances in theory and instrumentation, it is currently common practice to quantify net ecosystem fluxes using the eddy covariance (EC) technique because it provides continuous data that is integrated at the ecosystem scale (Baldocchi, 2003). Ecosystem flux studies, where CO_2 and CH_4 are measured in situ by EC, show that many wetlands are net GHG sources (over 20–100-year timescales) due to CH_4 emissions (Baldocchi, 2014). Whole ecosystem flux measurements, made using the EC technique, record the net result of all CH_4 and CO_2 production and consumption processes operating within the flux-footprint area for a given ecosystem. It is useful, therefore, to combine EC flux measurements with chamber techniques to gain insight into all the production and consumption processes that contribute to the net flux of CH_4 and CO_2 from an ecosystem (Covey and Megonigal, 2019).

Frank Lake is a natural wetland complex in southern Alberta (White and Bayley, 1999). When it is flooded, it has been the most important wetland in southwestern Alberta for nesting and staging waterfowl, marsh birds, and shorebirds (Sadler *et al.,* 1995). Before restoration, Frank Lake faced notable water level fluctuations and altered plant productivity due to natural climate variations and agricultural drainage (Sadler *et al.*, 1995; White and Bayley, 1999). Ducks Unlimited Canada (DUC) and other wildlife organizations have been aware of the ecological importance of the Frank Lake region for an extended period (Sadler *et al.*, 1995). Frank Lake was flooded in

1952 due to excessive runoff. Therefore, a drainage canal was excavated (Figure 2.1), which resulted in the partial drainage of the south basin, now recognized as Basin 3 (Sadler *et al.*, 1995). From 1983 to 1989, Frank Lake experienced dry conditions (Sadler *et al.*, 1995). As a result, in 1989, DUC initiated restoration efforts, utilizing wastewater effluent from a nearby town and a meat processing plant (Zhu *et al.*, 2019). The restoration aimed to establish and preserve premium waterfowl habitat, enhancing the biodiversity of the area. Simultaneously, it sought to offer supplementary treatment for the wastewater effluent entering Frank Lake (White and Bayley, 1999). The freshwater mineral-soil wetland at Frank Lake provides an ideal ecosystem to study the balance between CO_2 and CH_4 fluxes and to investigate the diverse biological and environmental controls that drive CO_2 and CH_4 fluxes in a restored freshwater mineral-soil wetland.

1.2 Research objectives

The primary goal of the proposed thesis research is to determine whether the Frank Lake wetland (Basin 3 East section-FLB3E) is a net sink or source of carbon by considering exchange processes that involve both CO_2 and CH_4. I addressed a series of research objectives as described below.

1. To determine the sink/source status of the ecosystem for CO_2 exchanges during the May-September growing season. The sink/source status of an ecosystem for CO_2 is calculated by measuring the net ecosystem exchange (NEE) of an ecosystem, which in turn represents the difference between C uptake in photosynthesis by plants and C loss in respiration by all organisms in an ecosystem. This study also aims to determine how diurnal and seasonal

changes in biological and environmental factors affect ecosystem CO_2 NEE measurements.

2. To determine the sink/source status of the ecosystem for CH_4 exchanges during the May-September growing season. Ecosystem CH_4 uptake can occur via CH_4 oxidation that is conducted by methanotrophic bacteria that function in aerobic soils. The amount of CH_4 taken up by methanotrophic bacteria is normally offset by CH_4 production and emission that results from the activities of methanogenic archaea organisms that live and function in anaerobic environments that are typically present in the flooded soils that regularly occur in freshwater mineral wetlands. This study also aims to determine how diurnal and seasonal changes in biological and environmental factors affect ecosystem CH_4 NEE measurements.

3. To calculate the net sustained global warming potential resulting from both CO_2 and CH_4 net exchange rates, where these calculations consider the various effects of CO_2 and CH_4 as greenhouse gases on a per molecule basis as well as the various lifetimes of the two gases in the atmosphere. With the use of these observations and calculations, it will be established whether the Frank Lake wetland (Basin 3 East) is a net source or sink for the combined impacts of CO_2 and CH_4.

CHAPTER 2: METHODS

2.1 Study site description

2.1.1 Introduction and location

Frank Lake is a prairie pothole wetland, a type of glacial remnant depressional wetland characteristic of the northern Great Plains (Bansal *et al.*, 2023). It acts as a vital staging area for migratory birds. Located 6 km east of the town of High River, Alberta, Canada (Latitude: 50.567. N; Longitude: 113.708. W), it encompasses 1262 hectares, with three main basins—Basins 1, 2, and 3—where Basin 3 is subdivided into North, West, and East sections (Figure 2.1). Prior to the restoration efforts led by Ducks Unlimited Canada (DUC) in 1989, Frank Lake experienced notable fluctuations in water levels and associated shifts in plant productivity, influenced by natural climate variations (Sadler *et al.,* 1995; White and Bayley, 1999). Ducks Unlimited Canada (DUC) restored Frank Lake wetland complex in 1989 for increased bird habitat, using treated industrial wastewater effluent from the town of High River (sewage treatment facility) and Cargill Foods meat processing facility (White and Bayley, 1999, 2001; Zhu *et al.,* 2019). The focus of this study was Basin 3 East (~40 ha) of the Frank Lake wetland complex, where the aquatic emergent plant, hardstem bulrush, *Schoenoplectus acutus*, (Muhl. ex Bigelow) exhibits expansive growth.

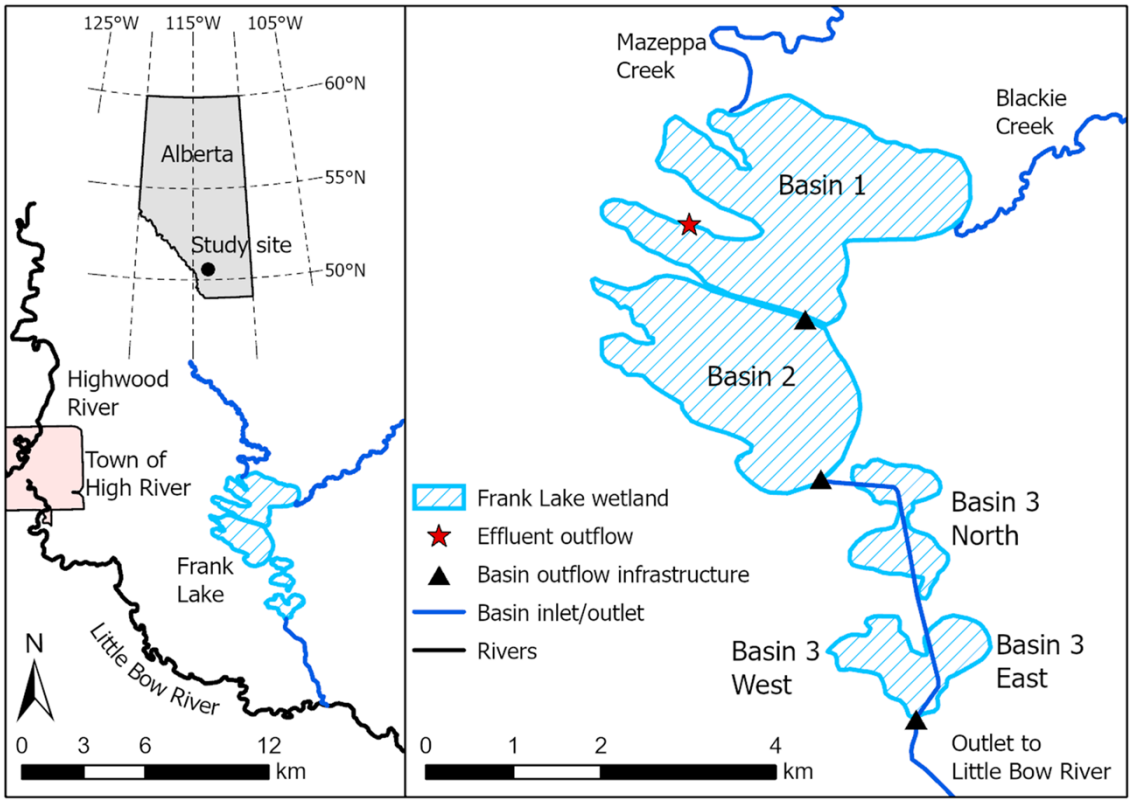

Figure 2.1: Map of the Frank Lake Wetland Complex, Alberta (Flanagan *et al.*, 2022)

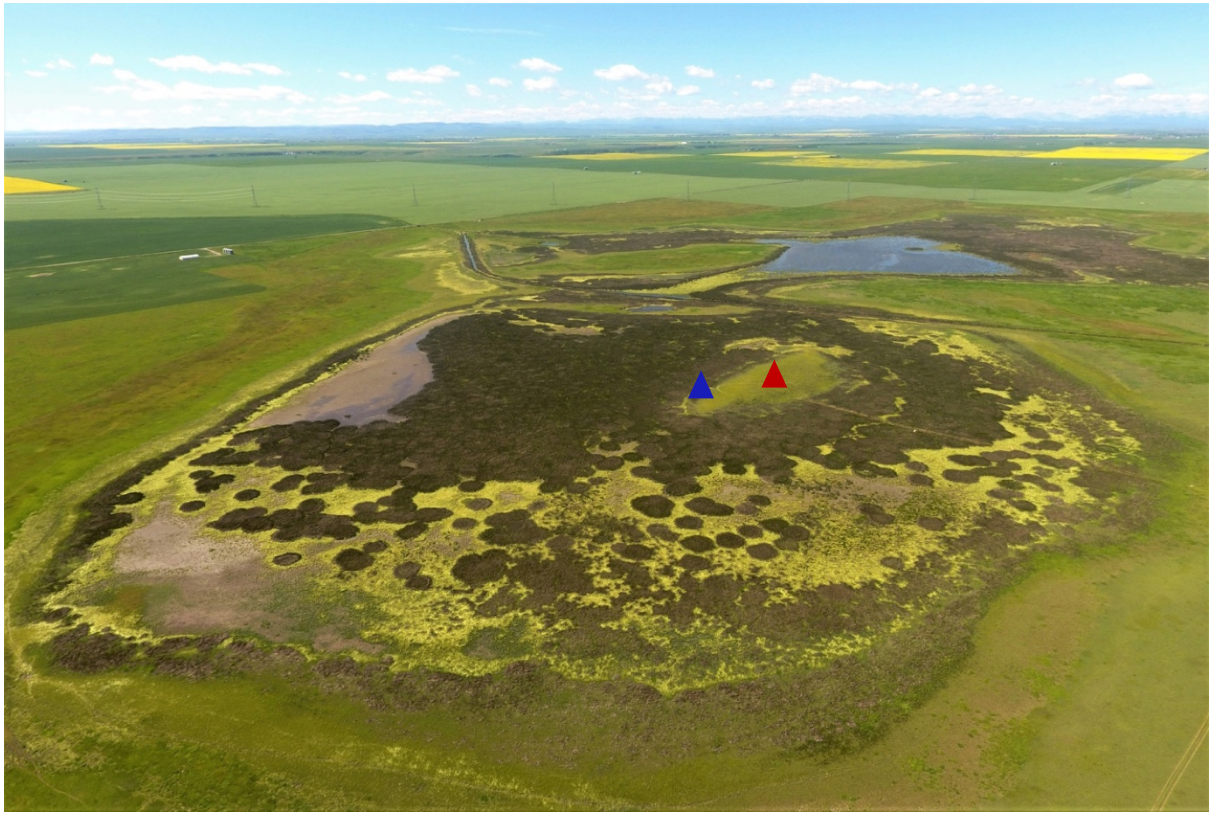

Figure 2.2: Drone photograph of Frank Lake Basin 3 East. (Photo Credit: Dr. Stewart Rood). The triangle in red represents the location of the eddy covariance tower and the triangle in blue represents the location of the meteorological instrumentation tower.

2.1.2 Climate and hydrology

The climate of Frank Lake is typical of the semi-arid Canadian prairies, with cold winters and warm summers (Zhu *et al.,* 2019). The recorded total precipitation at FLB3E during the main growing season months (May–September) of 2022, was 256 mm, while the average temperature was 14.5°C. In comparison, the long-term (1961-2018) averages recorded at the Blackie weather station (Blackie ACGM, Latitude: 50.5458. N, Longitude: 113.6403. W, www.acis.alberta.ca), showed a total precipitation of 298 mm and an average temperature of 13.2°C, during the main growing season months (May–September). Therefore, the growing season of 2022 in Frank Lake was relatively warmer and drier than the long-term average recorded at the Blackie weather station.

The wastewater effluent enters Frank Lake Basin 1 at an outlet of the combined pipeline from High River and the Cargill meat processing plant. Two ephemeral creeks (Blackie and Mazeppa) also discharge water to Frank Lake during the spring (Zhu *et al.,* 2019). Control weirs are present at the outlet points of the three main basins and a constructed drainage canal directs water flow from Basin 2 through Basin 3 and on to a coulee that drains into the Little Bow River (White and Bayley, 1999; Zhu *et al.,* 2019).

2.1.3 Vegetation

The dominant emergent aquatic vegetation in the Frank Lake wetland Basin 3 East was primarily composed of *Schoenoplectus acutus*, commonly known as hard stem

bulrush or great bulrush. *Schoenoplectus acutus* exhibited much more extensive coverage in Basin 3, specifically Basin 3 East. The expansive growth in Basin 3 East is attributed to a lower average water table depth (0.2 m) compared to Basins 1 and 2 (0.8 m), where the plant is typically confined to the periphery of open water zones (Native Plant Solutions, 2021).

2.1.4 Land use

This site was grazed by cattle from 19th July to the end of the measurement period (30th September 2022).

2.2 Vegetation sampling and monitoring

To determine the seasonal growth cycle of leaf area of the emergent aquatic plant *S. acutus*, the normalized difference vegetation index (NDVI), which is one of the most extensively applied vegetation indices related to leaf area index (LAI) and primary production (Wang *et al.,* 2005), was calculated. Normalized difference vegetation index (NDVI) was measured using two NDVI sensors (one upward looking - S2-111-SS, Apogee, Logan, UT, USA, and one downward looking - S2-112-SS, Apogee), monitoring a footprint of approximately 9 m^2. The sensors were mounted in the meteorological instrumentation tower (described in section 2.4) at 3 m height above ground. These sensors measure incoming and outgoing near infra-red (NIR) and red (RED) regions of the radiation wavelength spectrum, with the sensors having spectral ranges of 650 ± 5 nm (Red) and 810 ± 5 nm with 65 nm full-width half-maximum (NIR). The following equation (Equation 1) was used to calculate the NDVI, where NIR and

RED represents the reflectance values in specific wavebands for NIR and RED regions respectively.

$$NDVI = \frac{NIR - RED}{NIR + RED} \quad (1)$$

To provide perspective on the seasonal growth of *S. acutus* in 2022 compared to other recent years, NDVI values for the entire 2013–2021 time period calculated by Flanagan *et al.,* (2022) from Landsat reflectance measurements (monitoring a footprint of approximately 110,000 m^2) made in the area of extensive *S. acutus* vegetation at Basin 3 East were used.

During the peak of the growing season of 2022, bulrushes were harvested on day 221 and 227 for LAI determination. The sample collection of aboveground biomass samples of *S. acutus* was designed to provide broad coverage across the total area of the Basin 3 of the Frank Lake wetland complex, to account for the spatial heterogeneity in bulrush growth, and was timed to coincide with the approximate peak in the measured NDVI at the site. The coordinates of the eight sampling locations are provided in Appendix 1 and destructive sampling of bulrushes was done using four 20 cm * 50 cm quadrats in each location. The number of culms in each quadrat were recorded along with the basal area and the length of culms. Leaf area index of bulrushes was calculated based on the surface area of the bulrush stems which are assumed to be conical shaped. These measurements were used to calculate the total surface area of culms in each quadrat. Leaf area index was computed as the total area of green culms per area of ground (m^2 m^{-2}). The following equations were used to calculate the LAI

(m^2 m^{-2}) where LA_s is the leaf area of a single culm (m^2), n is the number of culms per quadrat, LA_T is the total leaf area, r is the average radius at the base of a bulrush culm (m), h is the average height of a bulrush culm (m), GA is the ground area (m^2), l is the length of the quadrat (m), and w is the width of the quadrat (m).

Single Leaf area (LA_s, m^2):

$$LA_s = \pi r^2 + \pi r(\sqrt{r^2 + h^2}) \quad (2)$$

Total leaf area (LA_T, m^2):

$$LA_s * n \quad (3)$$

Ground area (m^2):

$$GA = l * w \quad (4)$$

Leaf Area Index (m^2 m^{-2}):

$$LAI = \frac{\text{TOTAL LEAF AREA}}{\text{GROUND AREA}} \quad (5)$$

2.3 Eddy Covariance measurements

The net ecosystem fluxes of CO_2, CH_4, latent heat, and sensible heat were measured using the eddy covariance technique (Baldocchi, 2014), from 15th May to 30th September 2022, with equipment mounted on a 4.5 m tall aluminum instrumentation tower (Figure 2.3). A three-dimensional sonic anemometer (HS-R3, Gill Instruments, Limington, UK) was used to measure wind velocity, wind direction and temperature fluctuations. Two fast response, open path gas analyzers were used to measure the

atmospheric concentrations of methane (LI-7700, LI-COR, Lincoln, NE, USA), CO_2 and water vapor (LI-7500, LI-COR). Signals from the sonic anemometer and gas analyzers were sampled at a frequency of 10 Hz by the associated LI-COR Analyzer Interface Unit and recorded on a storage drive. Power was supplied to the eddy covariance sensors by an array of 6 V deep-cycle batteries that were charged by solar panels. The flux tower was located on an island near the center of the Basin 3 East of Frank Lake (Figure 2.2) where extensive ground coverage of *S. acutus* occurred, and there was flat, uniform fetch of c. 200 m in all directions surrounding the EC tower. Processing of high-frequency eddy flux was performed with EDDYPRO software (v7.0.9, LI-COR).

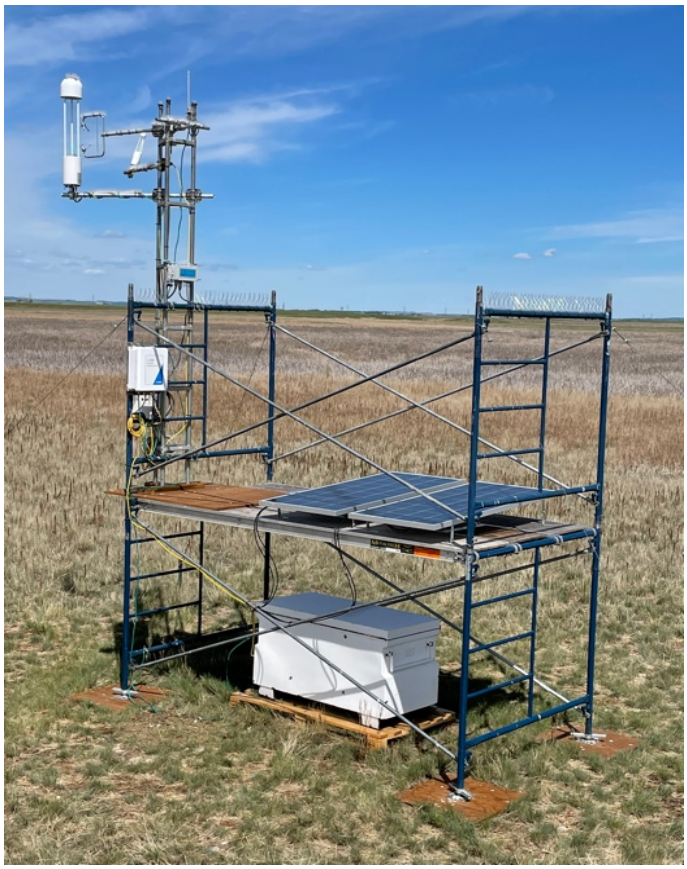

Figure 2.3: The eddy covariance system at Basin 3 East of Frank Lake, AB, wetland complex.

2.3.1 Evaluation of eddy covariance measurements

The evaluation of the surface energy balance closure (EBC) is an objective criterion in assessing eddy covariance data quality within the micrometeorological community (Barr *et al.,* 2006). The surface energy balance is closed when the energy flux into a system is equal to the energy flux leaving the system, plus any energy storage change in the system (Kidston *et al.,* 2010).

Energy balance closure (EBC) was calculated using equation 6;

$$\mathrm{EBC} = \frac{(\mathrm{H} + \mathrm{LE})}{(\mathrm{NR} - \mathrm{SHF})} \quad (6)$$

where NR is the net radiation flux density (Wm^{-2}), H is the sensible heat flux density (Wm^{-2}), LE is the latent heat flux density (Wm^{-2}), SHF is the heat flux density into the soil surface (Wm^{-2}). The sum of the turbulent fluxes in the numerator is the total turbulent heat flux and the denominator shows the difference between net radiation flux density and heat flux density, also called 'available energy'.

I evaluated the surface energy balance closure at FLB3E during the growing season of 2022 (day 137-273), using EC measurements of LE and H obtained from the EC tower and NR and SHF from the sensors in the meteorological tower.

2.4 Meteorological and environmental measurements

Throughout the 2022 growing season, meteorological variables were measured simultaneously with the fluxes using sensors mounted on an instrumentation tower (Figure 2.4) located 30 m from the EC flux tower (Figure 2.2). Air temperature and relative humidity were measured with a temperature and relative humidity probe (HMP45C, Campbell Scientific, Logan, UT, USA) located within a naturally ventilated radiation shield, mounted at a height of 2 m above ground. Net radiation was measured at a height of 3 m by a net radiometer (NR-LITE2, Campbell Scientific). Incoming photosynthetically active photon flux density (PPFD) was measured with a quantum sensor (LI190SB, LI-COR). Soil temperature, soil volumetric water content and soil electric conductivity was measured at three different locations close to the meteorological tower using probes (HydraProbe, Stevens) buried in soil at 15 cm depth. Soil heat flux (5 cm depth) was measured at three locations adjacent to the HydraProbes using soil heat flux plates (HFT3, Campbell Scientific). Soil water potential was measured using 2 soil water potential sensors located at 15 cm depth (TEROS 21, METER, Pullman, WA, USA). All meteorological data were collected by a datalogger (CR1000X, Campbell Scientific, USA) located in a fiberglass enclosure. Except for the rain gauge, all meteorological sensors were scanned at 60-s intervals and recorded as half-hourly means by the data logger. A tipping-bucket rain gauge (CS700, Campbell Scientific) was used to measure total precipitation recorded in 30-min intervals.

Figure 2.4: The meteorological instrumentation station at Basin 3 East of Frank Lake, AB, wetland complex.

2.5 Data handling and processing

2.5.1 Data quality control for CO_2 NEE dataset

A storage flux term is commonly incorporated into the calculation of CO_2 NEE (NEE = eddy flux + storage flux) in many studies (Long *et al.,* 2010; Bonneville *et al.,* 2008). However, at our study site, a storage flux was not included for the CO_2 eddy fluxes due to its negligible magnitude. In addition, the inclusion of the storage flux introduced additional noise into the CO_2 NEE dataset. Consequently, the CO_2 eddy flux alone was considered representative of CO_2 NEE.

During data processing, any instances where the CO_2 quality signal from the LI-7500 analyzer fell below 90% were identified and removed, leading to the removal of approximately 9% of the half-hourly data. Additionally, data points corresponding to periods of rainfall and instrument maintenance were excluded, accounting for the removal of approximately 0.8% of the CO_2 flux dataset. To identify extreme outliers, observations exceeding 3 standard deviations from the mean value were flagged and subsequently removed, amounting to approximately 1% of the half-hourly CO_2 flux data. These data filtering procedures were implemented to ensure the integrity and reliability of the CO_2 NEE dataset.

Furthermore, to ensure reliable measurements of flux using the eddy covariance technique, it is important to screen the data and remove periods with inadequate turbulence. To establish the threshold value of friction velocity (u*) required for acceptable CO_2 flux measurements, we conducted an analysis discussed below. This analysis involved evaluating the relationship between u* and CO_2 eddy flux using night-time-only data (PPFD < 5 $\mu mol\ m^{-2}\ s^{-1}$) obtained over the period from 11th July to 14th August, which corresponded to the peak NDVI.

To establish the u* threshold for the CO_2 dataset, I rank ordered the CO_2 NEE measurements (totaling 521 data points) by u* and divided them into ten roughly equal-sized groups. Each group represented 10% of the dataset. As a result, nine bins contained 52 measurements each, while one bin held 53 measurements. For each group, the average u* and average CO_2 eddy flux were calculated and plotted to assess the relationship between CO_2 flux and u* (Figure 2.5). The resulting graph exhibited

a curvilinear pattern, without a clear sharp break from linear response to a plateau. However, there was a slight plateauing observed around a u* value of 0.12 m s^{-1}.

To further investigate whether the plateauing occurred around 0.12 m s^{-1}, a segmented linear regression analysis was conducted. This analysis divided the data into two sections: a section showing a positive linear response (first six points of Figure 2.5) and a section exhibiting a flat plateau (last four points of Figure 2.5), both containing the data point corresponding to 0.12 m s^{-1}. The regression of the first six points showed a strong linear relationship (Figure 2.5, r^2=0.848, $p<0.05$) as shown by the red dashed line, while the regression of the last four points demonstrated a non-significant relationship with a slope not different from zero (Figure 2.5, r^2=0.192, $p>0.05$), indicating the presence of a plateau. Based on these findings, the u* threshold value for screening the data was determined as 0.12 m s^{-1}. This u* threshold value of 0.12 ms^{-1} was selected as the point where an increase in turbulence no longer significantly increased nighttime CO_2 flux. The u* screening method was then applied, leading to the removal of all CO_2 flux data (~25% of the dataset) associated with u* values below 0.12 m s^{-1}. Overall, all flux quality control procedures resulted in the removal of ~36% of the possible half-hourly CO_2 NEE data collected between May and September 2022, so 64% of the data remained for further analyses.

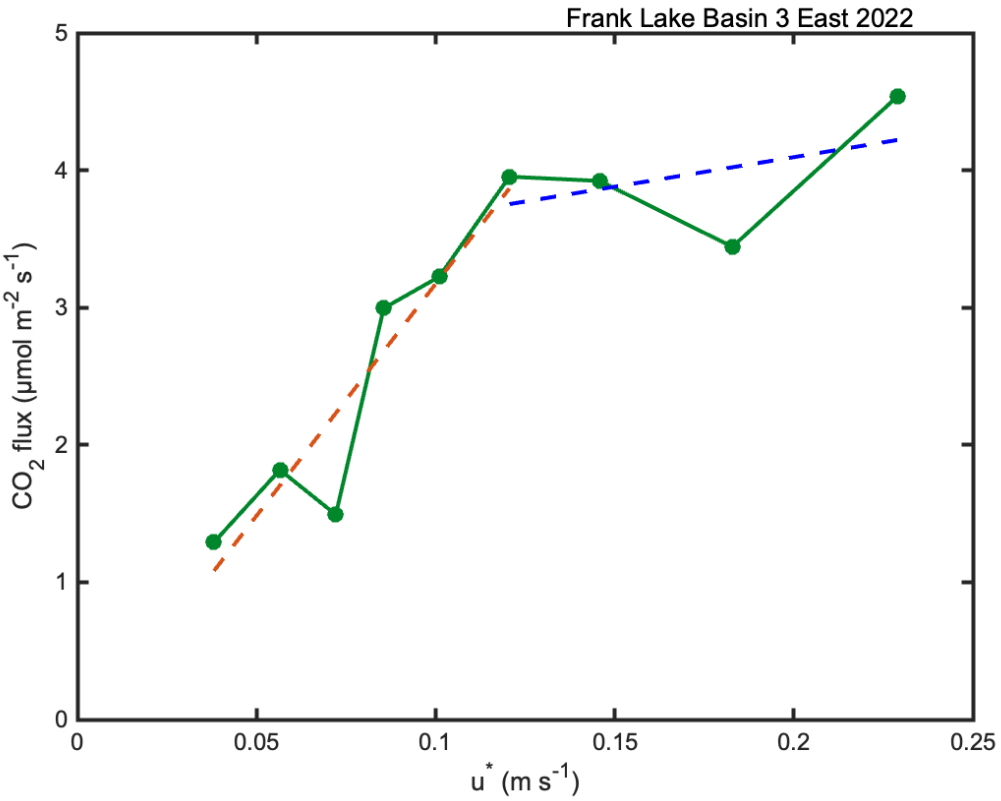

Figure 2.5: The relationship between friction velocity (u*) and nighttime CO_2 NEE for the growing season of 2022 at Frank Lake Basin 3 East. For this purpose, data were rank ordered and grouped by u*, with each data point representing roughly 10 % of the total half-hourly CO_2 flux data. Total number of data points was 521, where nine bins contained 52 measurements each, while one bin held 53 measurements. The red dashed line shows the linear regression between u* and first six points (r^2=0.848, $p<0.05$) and the blue dashed line shows the linear regression between u* and last four points (r^2=0.192, $p>0.05$).

2.5.2 Data quality control for CH_4 NEE dataset

In contrast to the CO_2 flux measurements, the CH_4 eddy fluxes were subjected to the inclusion of a storage flux term for the determination of net ecosystem exchange (NEE), using the equation NEE = eddy flux + storage flux. To ensure the reliability of CH_4 flux measurements, several data removal procedures were implemented. First, CH_4 NEE data were excluded when the Received Signal Strength Indicator (RSSI) of the LI-7700 analyzer dropped below 20%. Approximately 25% of the CH_4 NEE data were removed due to this criterion. Furthermore, CH_4 flux data were eliminated during periods of rain and instrument maintenance, accounting for approximately 1% of the data removal. To identify extreme outliers in the CH_4 NEE flux data, observations exceeding 3 standard deviations from the mean value were flagged. Approximately 1% of the dataset were identified as outliers and subsequently removed from the analysis.

Similarly, to the approach used for the CO_2 flux data, I applied a u* threshold to the CH_4 net ecosystem exchange (NEE) data for turbulence screening. The same u* threshold value of 0.12 m s^{-1} that had been determined for the CO_2 flux data was also applied to the CH_4 flux data. Applying the u* screening to the CH_4 flux data resulted in the identification and subsequent removal of approximately 19% of the available half-hourly data recorded between May and September 2022. Overall, these four procedures resulted in the removal of 46% of the possible half-hourly CH_4 NEE data collected between May and September 2022, leaving 54% of the CH_4 NEE data for further analyses.

2.5.3 Gap filling CO_2 NEE dataset

To fill gaps in the CO_2 dataset, I computed mean diurnal patterns for NEE, PPFD, and air temperature (T) for approximately 2-week intervals, after carrying out the data quality control procedures as described in the section 2.5.1. These patterns were obtained by calculating bin-averages based on time of day, covering approximately 15-day periods during the study period from May to September 2022. Data from the mean diurnal trends were then fitted to the following equation:

$$NEE = -\frac{A_{max}\alpha PPFD}{A_{max} + \alpha PPFD} + R_{10}Q_{10}^{\left(\frac{T-10}{10}\right)} \quad (7)$$

where A_{max} is the maximum gross ecosystem photosynthesis (μmol m^{-2} s^{-1}) at infinite PPFD (μmol m^{-2} s^{-1}); α is the initial slope of the ecosystem photosynthesis light-response curve (mol CO_2 mol $photons^{-1}$); R_{10} is total ecosystem respiration rate (TER) at 10 ^{0}C (μmol m^{-2} s^{-1}); Q_{10} is the temperature sensitivity coefficient for TER for a 10^{0}C change in temperature; and T is air temperature (^{0}C). Non-linear, least squares regressions were used to calculate estimates of A_{max}, α, R_{10} and Q_{10} parameters. The calculations were done with the parameters bound over the following ranges: A_{max} between 0.1 and 40, α between 0.025 and 0.06, R_{10} between 0.01 and 8.0, and Q_{10} between 1.8 and 2.2.

To gap-fill the net ecosystem exchange (NEE) data and determine the partitioning of NEE into gross ecosystem photosynthesis (GEP) and total ecosystem respiration (TER), Equation 7 was utilized in conjunction with meteorological measurements,

photosynthetic photon flux density (PPFD) and temperature (T). Equation 7 consists of two terms on the right-hand side: the first term represents GEP, while the second term represents TER.

The NEE, expressed as -GEP + TER, provided a measure of the net carbon exchange of the ecosystem. Negative NEE values indicated net CO_2 uptake by the ecosystem. I computed and presented the period-wise and growing season carbon budgets by considering the seasonal variations in each parameter (A_{max}, α, R_{10}, Q_{10}), which were determined through calculations performed on four chosen study periods (approximately 30-day intervals) during the growing season.

To estimate the growing season C budget, I integrated the available EC measurements with gap-filled data derived using Equation 7 when EC measurements were unavailable. By employing this methodology, I was able to derive robust growing season carbon budgets, considering both measured EC data and gap-filled data when necessary.

2.5.4 Gap filling CH_4 NEE dataset

To address the need for a rigorous method to gap fill the CH_4 NEE dataset, I conducted a comprehensive analysis, which revealed a distinct disparity between the daytime and nighttime CH_4 NEE values throughout the growing season of 2022. To begin with, I assessed the normality of the daytime and nighttime CH_4 NEE datasets using the Shapiro-Wilk test. The results indicated a departure from normal distribution in both cases. Consequently, a non-parametric Kruskal-Wallis test was employed to

determine the significance of the difference between mean values for the daytime and nighttime CH_4 NEE values. The Kruskal-Wallis test yielded a highly significant difference ($p<0.01$, Figure 2.6) between the daytime and nighttime CH_4 NEE datasets. As a result, relying on the daily average CH_4 NEE values for gap filling was deemed inappropriate.

Subsequently, I conducted an analysis to determine whether there was a seasonal trend in the daily average CH_4 NEE values separately for nighttime and daytime periods. To accomplish this, I computed the daily averages of CH_4 NEE for both daytime and nighttime periods and then fitted a second-order polynomial to each dataset to analyze seasonal variation in the daily average values. For the daytime CH_4 NEE values, there was a significant seasonal trend ($p<0.05$, Figure 2.7a), although the trend was only slightly increasing. In contrast, for the nighttime CH_4 NEE values, there was no significant seasonal trend ($p>0.05$, Figure 2.7b).

Furthermore, I examined the mean diurnal trend of CH_4 NEE over the 2022 growing season. To do this, I plotted the average CH_4 NEE values, binned by time of day, and fitted them with a fourth-order polynomial. There was a significant diurnal variation ($p<0.01$, Figure 2.8) for this dataset. Consequently, I utilized this mean diurnal pattern to fill in the gaps of missing CH_4 NEE values during the growing season of 2022.

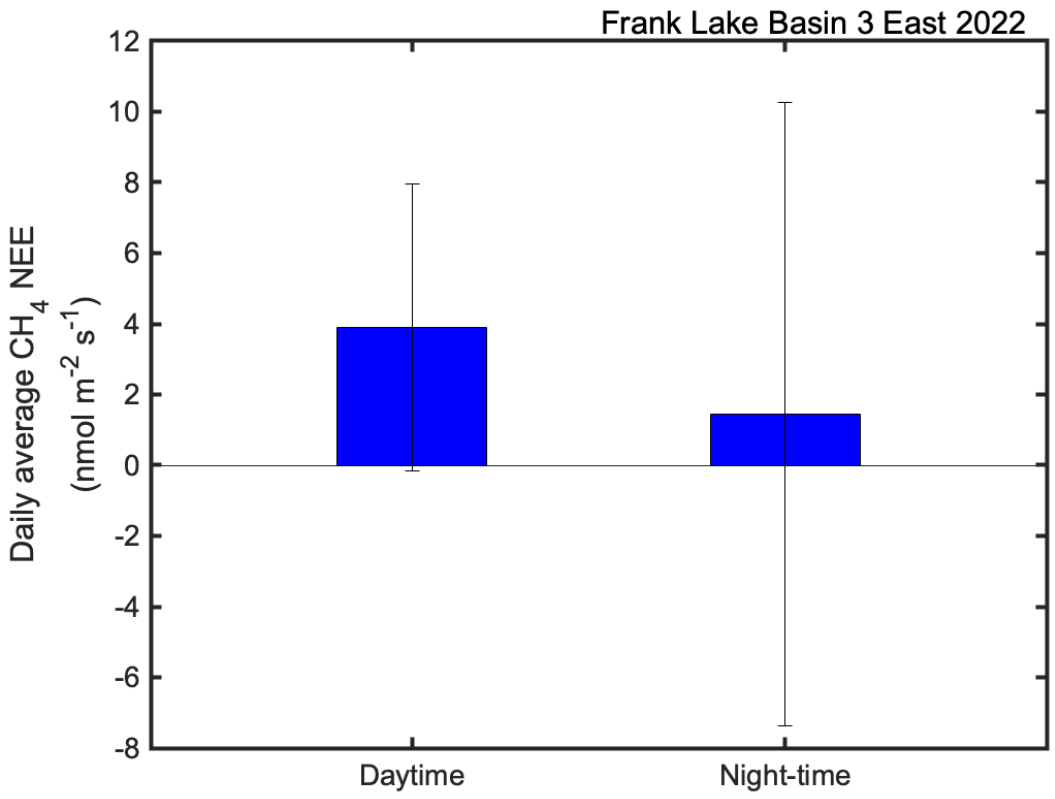

Figure 2.6: The difference between the daytime and night-time daily average CH_4 NEE (nmol m^{-2} s^{-1}) during the growing season of 2022 at Frank Lake Basin 3 East. Daily-average CH_4 NEE differed significantly between daytime and nighttime ($p<0.01$) based on the Kruskal-Wallis test.

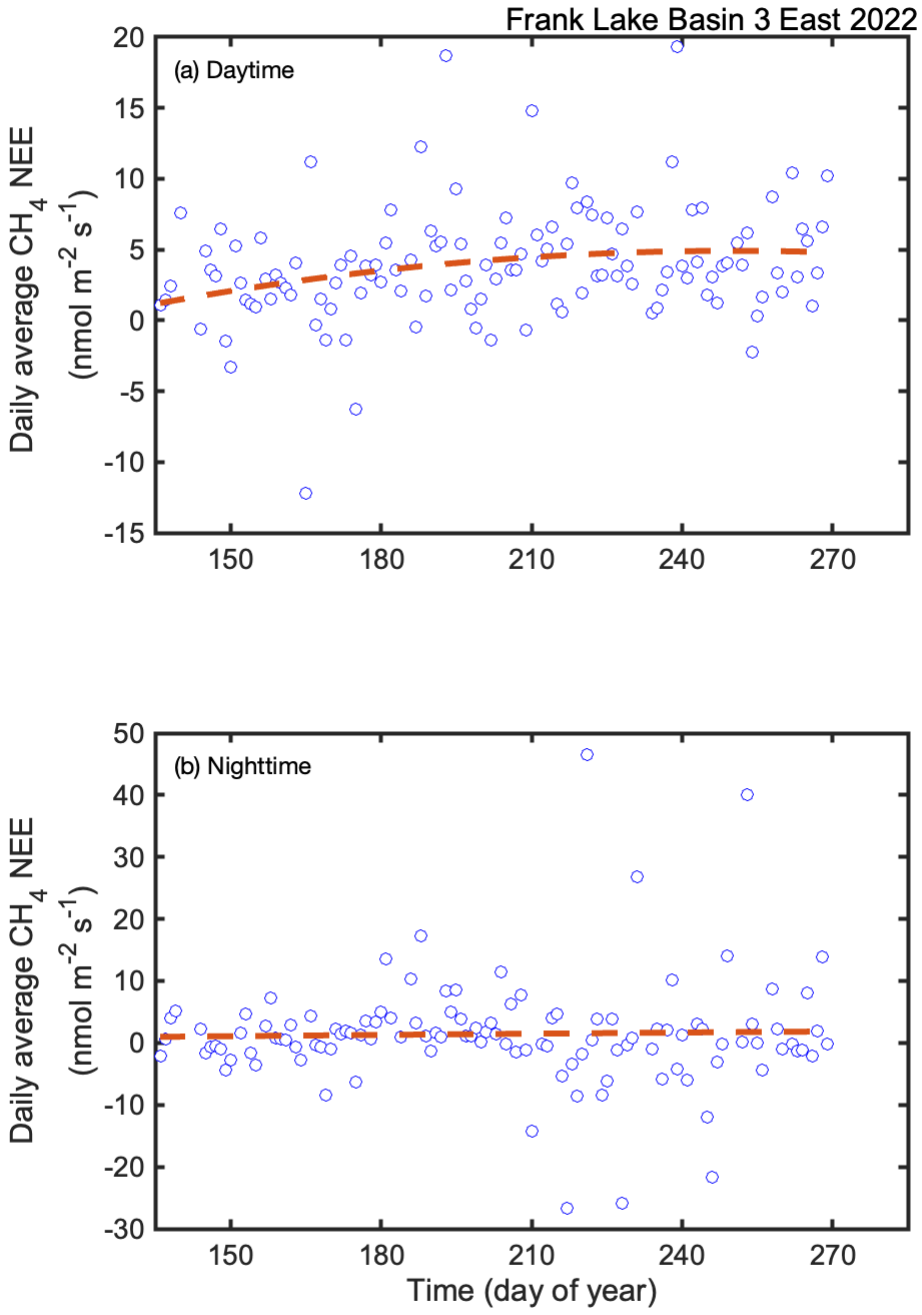

Figure 2.7: The seasonal trend of daytime and nighttime daily average CH_4 NEE as plotted by the day of year (DOY). A second-order polynomial curve is fitted to the daily average CH_4 NEE values (nmol m^{-2} s^{-1}) separately for (a) daytime and (b) nighttime datasets. There was no significant seasonal trend ($p>0.05$) for the nighttime CH_4 NEE values while there was a significant seasonal trend ($p<0.05$) for the daytime CH_4 NEE values.

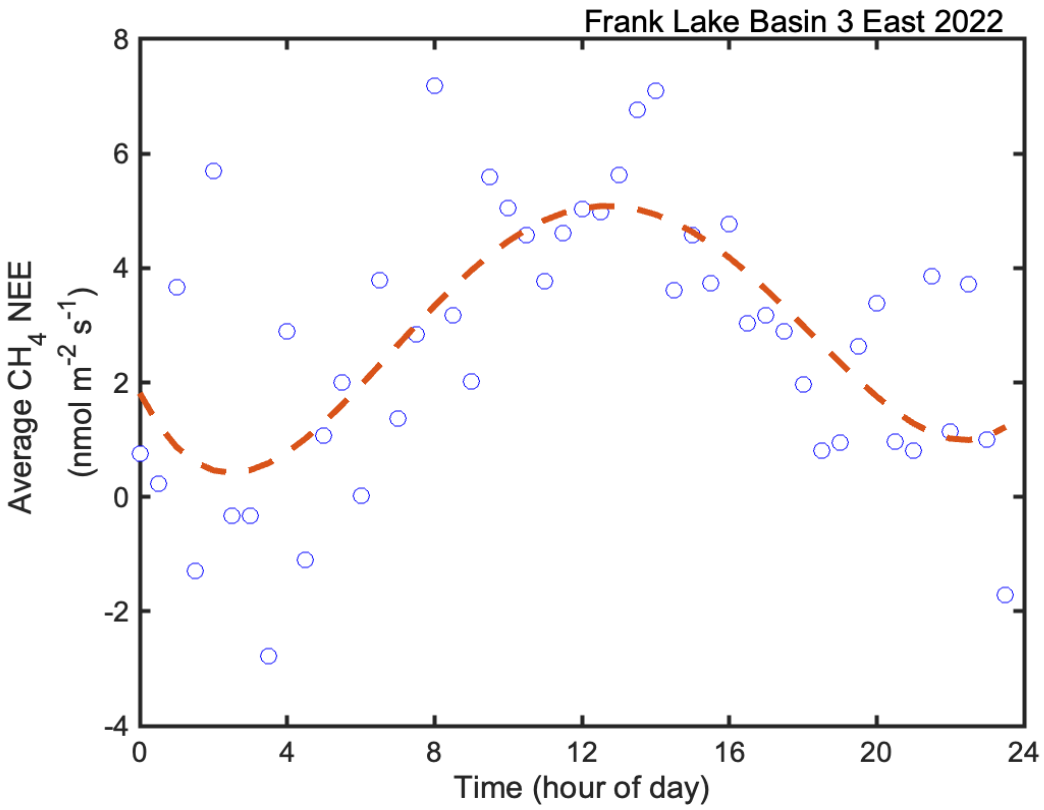

Figure 2.8: Diurnal pattern of average CH_4 NEE as plotted by hour of day. A fourth-order polynomial curve is fitted to the diurnal average CH_4 NEE values during the growing season of 2022 at Frank Lake Basin 3 East. The polynomial equation used for gap-filling is given in brackets ($y=4.43*10^{-4}x^4 - 0.02\,x^3 + 0.33\,x^2 - 1.25\,x + 1.81$, Adjusted $r^2=0.425$, $p<0.05$)

2.6 Global warming potentials and growing season carbon budget

A comparison between net CO_2 flux and net CH_4 flux was made for Frank Lake Basin 3 East in the 2022 growing season to determine if the wetland is a net source or sink of greenhouse gases. First, the daily-integrated fluxes of CH_4 and CO_2 were calculated after gap filling data for each period (time periods represent the following intervals: (1) Period 1 (days 136–166); (2) Period 2 (days 167–196); (3) Period 3 (days 197–227); (4) Period 4 (days 228–269). When fluxes are sustained over time, the emission of 1 kg CH_4 m^{-2} $year^{-1}$ would be offset by the persistent sequestration of 45 kg CO_2 m^{-2} $year^{-1}$ (Neubauer and Megonigal, 2015). Therefore, a multiplier of 45 (mass basis) was applied to CH_4 flux data, for a 100-year time horizon, to account for a larger warming effect of CH_4, when present within the atmosphere. With the application of this multiplier, CH_4 was then expressed in units of CO_2-equivalents, which allowed a direct comparison between CH_4 emission and CO_2 sequestration. Then, the seasonally-integrated fluxes were calculated for CO_2 and CH_4 to calculate the overall C budget. I use the term, sustained global warming potential (SGWP), to refer to the CH_4 net flux expressed in equivalent CO_2 units. A net SGWP flux was then calculated for Frank Lake Basin 3 East as the sum of the CH_4 SGWP flux and the CO_2 flux.

2.7 Statistical Analysis

All the statistical tests and model fittings including the parameter estimation in the CO_2 NEE partitioning was conducted using MATLAB (R2022a, The MathWorks Inc). The linear regressions of fluxes and environmental and biotic factors were conducted using the 'lm' function in MATLAB.

CHAPTER 3: RESULTS

3.1 Evaluation of eddy covariance measurements

During the growing season of 2022, the relationship between available energy (net radiation-storage heat flux) and the sum of turbulent heat fluxes (Latent heat flux (LE)+ Sensible heat flux (H)), was significant for Frank Lake Basin 3 East ($r^2 = 0.88$, $p<0.05$). However, the slope of the regression between the available energy and the sum of turbulent heat fluxes was less than 1 (88%). Studies have reported that turbulent energy fluxes are frequently (but not always) underestimated by about 10–30% relative to estimates of available energy (Wilson *et al.,* 2002), which suggests that there is a good closure observed at FLB3E during the growing season of 2022. This result suggests that estimates of the scalar turbulent fluxes of sensible and LE are underestimated and/or that available energy is overestimated. The lack of energy balance closure could be in part attributed to sampling errors associated with different measurement source areas for turbulent heat fluxes, net radiation, and soil heat flux (Wilson *et al.,* 2002) because turbulent fluxes were measured from the eddy covariance instruments while the net radiation and soil heat flux are measured using sensors at the meteorological station located about 30 m from the eddy covariance flux tower. If the energy imbalance results from different measurement source areas, it is believed that there may be no reason to suspect that the measured fluxes are systematically inaccurate (Wilson *et al.,* 2002).

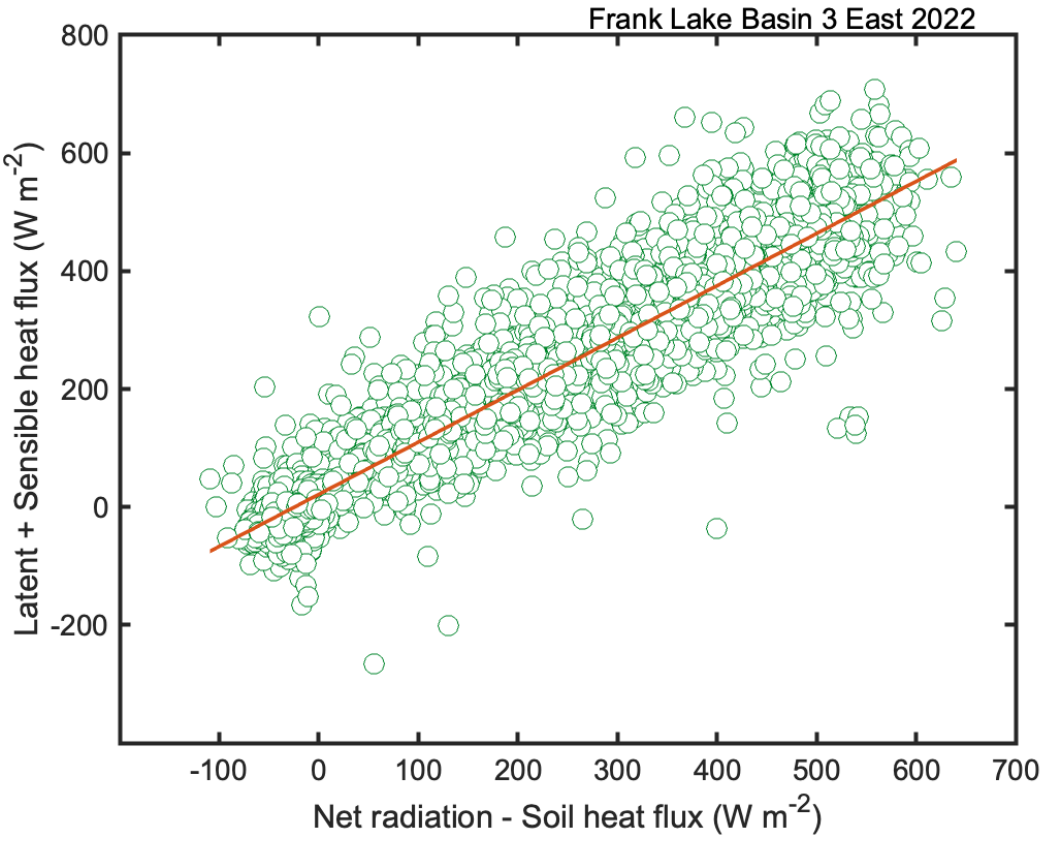

Figure 3.1: Energy balance closure for the half hourly eddy covariance measurements made at Frank Lake Basin 3 East during the growing season of 2022 (sensible and latent heat fluxes (y), available energy (x); $y = 0.88x + 21.44$, adjusted $r^2 = 0.88$, $n = 4302$, $p<0.05$).

3.2 Seasonal Variation in Greenness of Emergent Aquatic Vegetation

During a typical year, plant growth was initiated in early May (~ day 130), with peak values observed by mid-July (~ day 196) and sustained until mid-August (~ day 227). NDVI values then gradually declined, reaching their lowest values during mid-to-late October (days 288–93) (Figure 3.2). By contrast, in the relatively warm and dry year of 2022, tower based NDVI values exhibited a delayed start (~day 147), reached peak values (~day 218) with only a relatively short period at maximum NDVI (~20 days) and declined rapidly to reach the low values. The growing season length in 2022 was shorter (~130 days) compared to a typical year (~160 days). At the peak NDVI values observed during period 3, the leaf area index (LAI) measured (using quadrats sampled on day 221 and 227) was 2.25 ± 0.89 m^2 m^{-2}.

For the purposes of this study, the growing season of 2022 was categorized into four distinct periods based on NDVI values, which reflect different stages of plant phenology; period 1- days 136-166 (mid-May to mid-June) marked the early growth and leaf emergence of bulrush plants; period 2- 167-196 (mid-June to mid-July) represented a phase of rapid plant growth; period 3- 197-227 (mid-July to mid-August) indicated the peak of the growing season; period 4- 228-269 (mid-August to late September) characterized the late growth season and the initiation of plant senescence. These periods were important to examine seasonal variation among different types of data with each period having approximately equal numbers of half hourly measurements (close to monthly periods) and a large sample size to carry out rigorous analyses, as illustrated in Table 3.1.

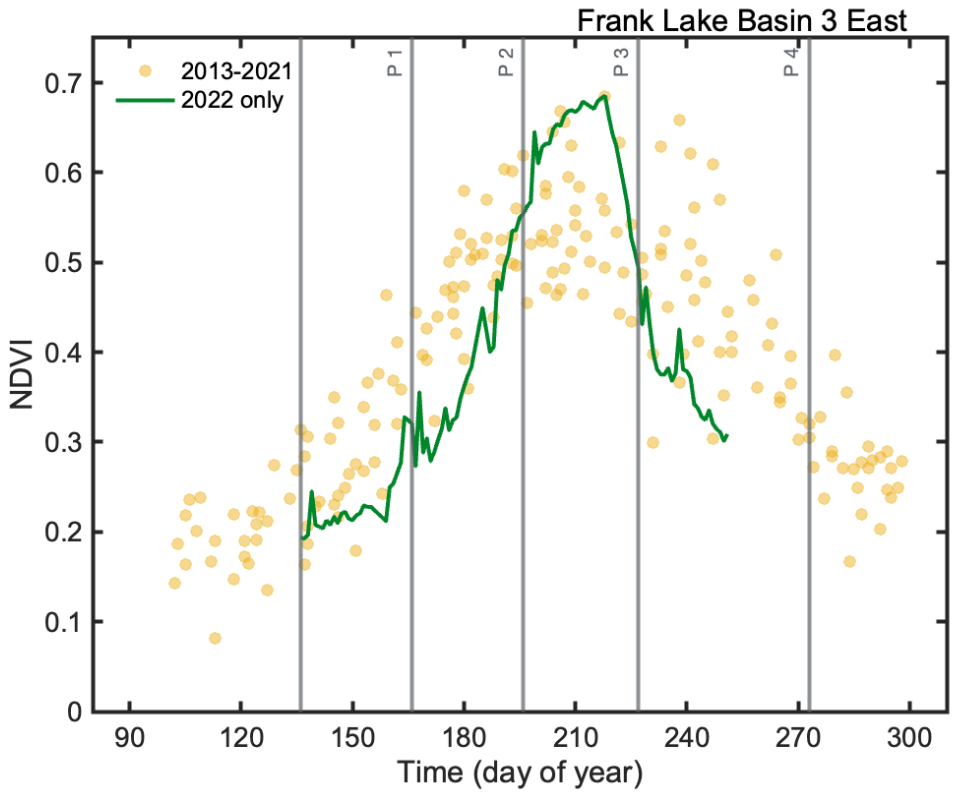

Figure 3.2: Seasonal variation in normalized difference vegetation index (NDVI). The data points represent values calculated from Landsat reflectance measurements made in the Frank Lake Basin 3 East marsh, an area dominated by *Schoenoplectus acutus* on specific days during 2013–2021 (Flanagan *et al.,* 2022). The green line represents measurements of NDVI from met mast NDVI instruments. The vertical grey lines were used to separate the four phenological periods (P1-P4).

Table 3.1: The whole growing season was divided into four phenologically different periods based on NDVI values labelled as period 1 to 4. The time frame, start date (DOY), end date (DOY) and the total number of days in each period are provided.

Period	Time frame	Start DOY	End DOY	Total days
Period 1	May 16 - Jun 15	136	166	31
Period 2	Jun 16 - Jul 15	167	196	30
Period 3	July 16 - Aug 15	197	227	31
Period 4	Aug 16 - Sep 30	228	273	46

3.3 Seasonal variation in environmental conditions

During the growing season of 2022, the air temperature increased from May to a peak in August, followed by a decline in September (Figure 3.3a). During the study period, the monthly average air temperatures displayed significant variation, with August recording the highest mean temperature (~18 ^{o}C) and May recording the lowest May (~9 ^{o}C). Except for May, the study site was characterized by warmer than long-term average monthly temperatures. In May, the mean monthly air temperature was near the long-term average air temperature. Additionally, soil temperature displayed a notable increase, starting at around 8 ^{o}C in early May, reaching peak values (~17 ^{o}C) by the end of July, and gradually declining throughout September (Figure 3.4a).

During the growing season of 2022 (May-September), the total precipitation in the FLB3E area (255.9 mm) was ~86% of the long-term average (298.1 mm), based on measurements taken from 1961-2018 at the nearby Blackie meteorological station

located near High River (Figure 3.3b). The study site experienced limited rainfall in May, August, and September in 2022, while precipitation in July was close to the long-term average. However, June witnessed significantly higher rainfall than the long-term average, with an excess of 53.5 mm, primarily due to a few intense rain events. It's important to highlight that the excess water from the June rain events was not efficiently retained in the soil. Figure 3.9 demonstrates that although a few substantial rain events that occurred earlier in June briefly increased soil moisture, subsequent rain events resulted in only marginal increases, regardless of their size. This pattern could be attributed to higher evaporation rates surpassing precipitation inputs, leading to a soil moisture deficit.

At the beginning of the growing season, the soil volumetric water content (soil VWC) measured at 15 cm depth (Figure 3.4c) started at ~0.4 m^3 m^{-3}, increased, and fluctuated around peak values of ~0.45 m^3 m^{-3} until the end of July. Due to relatively warmer and drier than long-term average conditions observed during the growing season of 2022, it resulted in an abrupt decline in the soil VWC in July, after which a gradual reduction was observed during the remaining months (August–September). According to Figure 3.4d, soil water potential remained near 0 kPa from May to end of July. A drastic decline in soil water potential was recorded during August and September, and soil water potential reached low values (~700 kPa), indicating that available soil moisture in the shallow soil layers (above 15 cm depth) in FLB3E during the growing season of 2022 was` largely exhausted by late July. Daily integrated PPFD values showed large fluctuations during the growing season of 2022 where it increased from low values in May (~30 mol m^{-2} day^{-1}) to peak values in late June (~60

mol m^{-2} day^{-1}) and declined to low values in late September (~30 mol m^{-2} day^{-1}) (Figure 3.4 b).

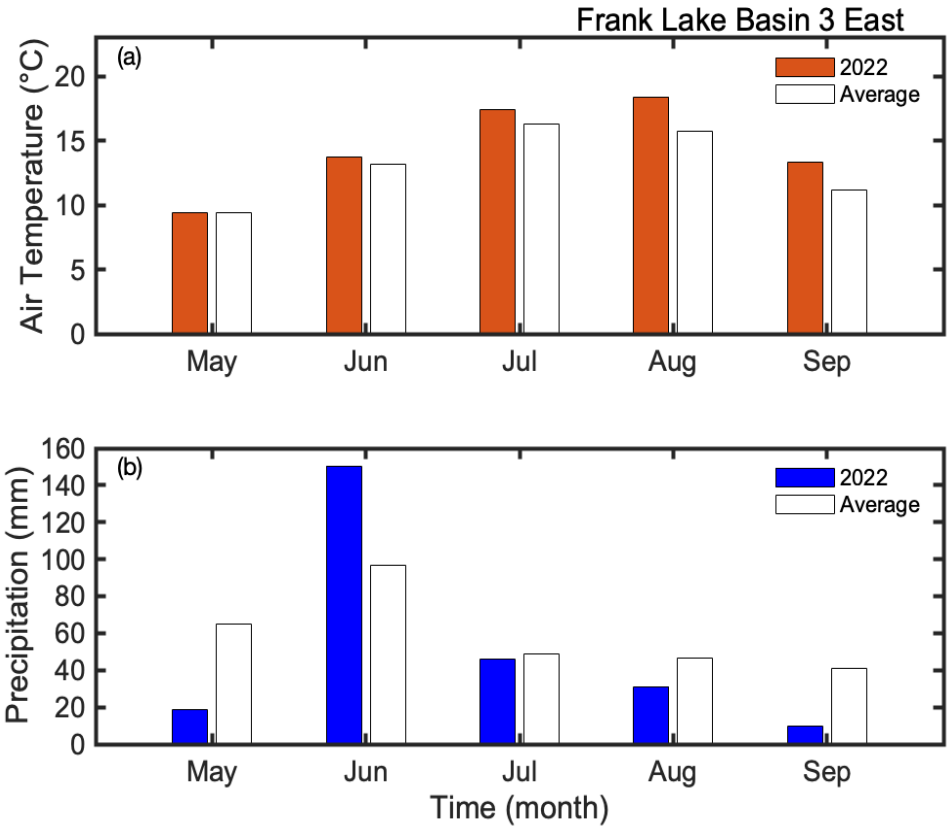

Figure 3.3: (a) The average monthly air temperature and (b) cumulative monthly precipitation recorded at Frank Lake Basin 3 East during the growing season of 2022 in comparison to the long-term average monthly temperature and precipitation recorded at the Blackie Met station (1961–2018), climate station that was used as an approximation for the climate normal in the study region.

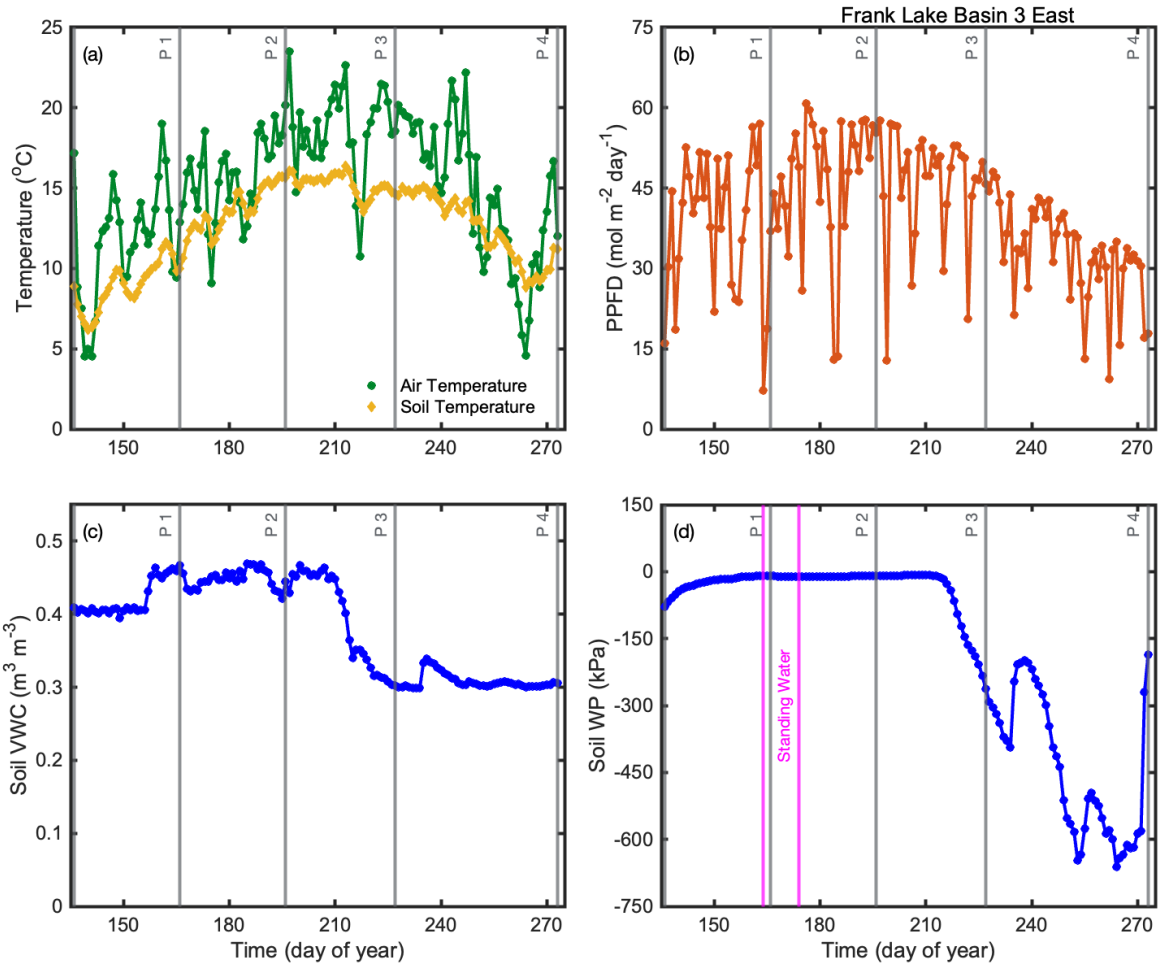

Figure 3.4: (a) Average daily air temperature and soil temperature (°C), (b) daily integrated photosynthetically active photon flux density (PPFD, mol m^{-2} day^{-1}), (c) daily average soil volumetric water content (Soil VWC, unitless) and (d) soil water potential (Soil WP, kPa). Soil VWC and Soil WP were measured at 15 cm depth. The vertical lines in pink represents the approximate duration where FLB3E had standing water. The vertical grey lines were used to separate the four phenological periods (P1-P4).

Table 3.2: Identification of growing season periods, including date ranges, descriptive characteristics, and corresponding environmental conditions. The environmental parameters considered were air temperature (^{o}C), soil temperature (^{o}C), soil volumetric water content (soil VWC, $m^3\ m^{-3}$), soil water potential (soil WP, kPa), daily-integrated photosynthetically active photon flux density (PPFD, mol $m^{-2}\ day^{-1}$).

Period	Period 1	Period 2	Period 3	Period 4
	(May 16 - Jun 15)	(Jun 16 - Jul 15)	(Jul 16 – Aug 15)	(Aug 16 – Sep 30)
Description	Bulrushes emerged, low NDVI, low NEE	Bulrushes growth increased rapidly, NDVI increased rapidly, NEE increased	Bulrush growth peaked, NDVI peaked, NEE plateaued	NDVI declined, most vegetation senesced, NEE decreased
Air temperature (^{o}C)	11.7±3.6	15.7±2.6	18.7±2.7	14.6±4.4
Soil temperature (^{o}C)	9.0±1.5	13.7±1.4	15.2±0.7	12.5±2.0
Soil VWC ($m^3\ m^{-3}$)	0.42±0.02	0.45±0.01	0.39±0.06	0.31±0.01
Soil water potential (kPa)	-25.2±18.0	-10.6±0.7	-61.6±81.2	-438.7±158.2
Daily integrated PPFD (mol $m^{-2}\ day^{-1}$)	38.1±13.1	46.8±12.5	46.0±10.6	32.9±8.8

Table 3.3: Analysis of differences among four phenological time periods for five environmental conditions. The environmental parameters considered were air temperature (°C), soil temperature (°C), soil volumetric water content (soil VWC, m^3 m^{-3}), soil water potential (soil WP, kPa), daily-integrated photosynthetically active photon flux density (PPFD, mol m^{-2} day^{-1}). The differences among the periods were based on One-way Analysis of Variance and subsequent Tukey Multiple Comparison Tests. P1-P4 represents the four phenological periods. Two symbols are used to represent p values, where * denotes ($p<0.05$) and ~ denotes ($p>0.05$). Cells highlighted in green represent cases where significant differences were observed. White cells represent cases where there were no significant differences observed.

Period pairing	P1 & P2	P1 & P3	P1 & P4	P2 & P3	P2 & P4	P3 & P4
Air temperature (°C)	*	*	*	*	~	*
Soil temperature (°C)	*	*	*	*	*	*
Soil VWC (m^3 m^{-3})	*	*	*	*	*	*
Soil water potential (kPa)	~	~	*	~	*	*
Daily integrated PPFD (mol m^{-2} day^{-1})	*	*	*	~	*	*

3.4 Sensible and latent heat exchange

During the growing season of 2022 at FLB3E, the ecosystem showed smooth mean diurnal patterns for latent and sensible heat fluxes calculated over roughly 30-day intervals that were driven by available energy input (Figure 3.5). The mean diurnal values of H exceeded LE during the start of the growing season (period 1), with mid-day Bowen ratios (BR=H/LE) greater than unity (Figure 3.5a). However, as the growing season progressed (period 2), mean diurnal values of LE surpassed those of H, and the mean BR dropped below unity for all times of the day (Figure 3.5b). During the peak growing season (period 3), the mean diurnal values of LE and H were almost equal, and the BR were near unity during mid-day (Period 3, Figure 3.5c). During late growing season (period 4) when the plants senesced, the H was greater than LE during mid-day (Figure 3.5d). The partitioning of turbulent heat fluxes at various plant phenological stages observed during this study indicated a robust seasonal trend and substantial regulation of these fluxes by plant phenology.

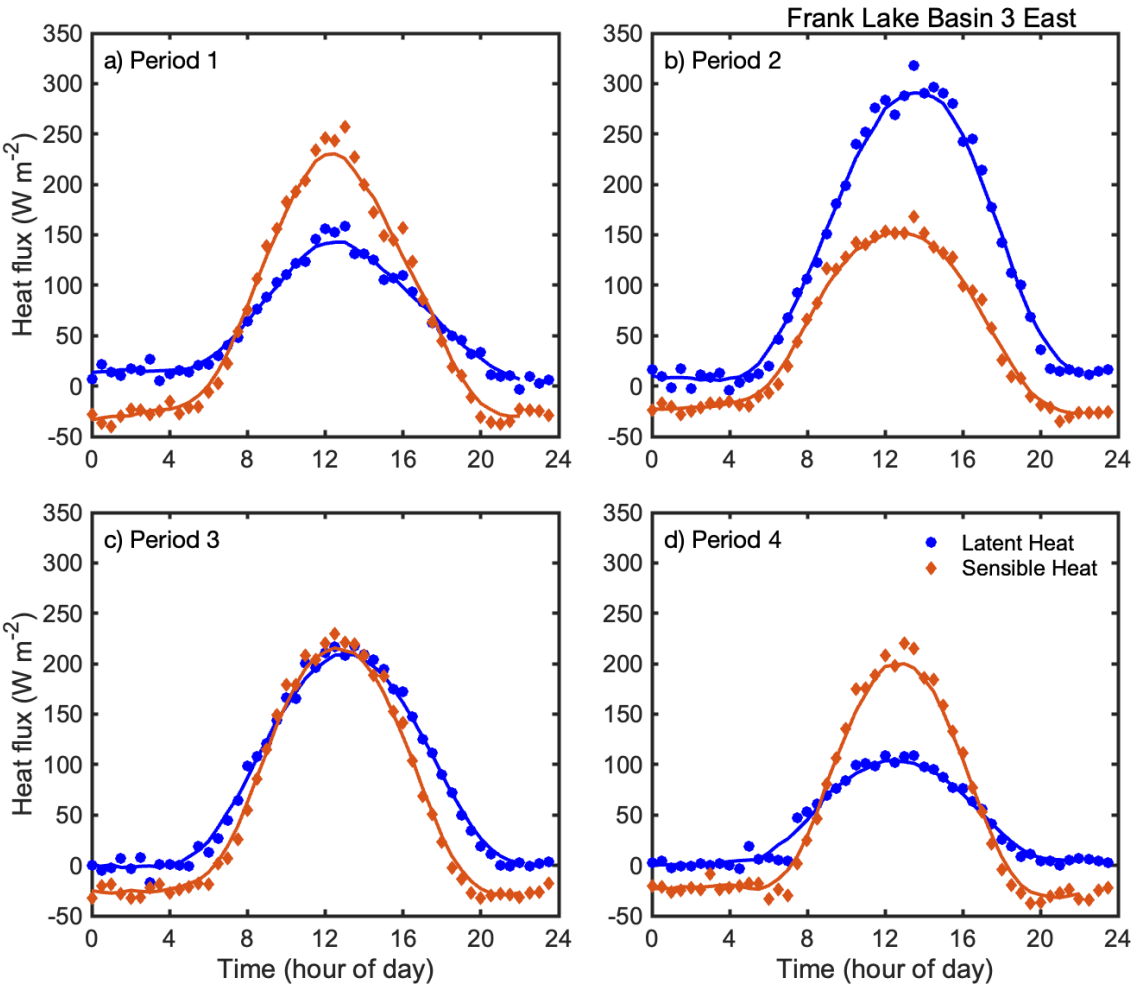

Figure 3.5: Mean diurnal trends of sensible (H; red diamonds) and latent (LE; blue dots) heat fluxes (Wm^{-2}) at the Basin 3 East of Frank Lake during the growing season of 2022. Time periods represent the following intervals: (a) 'Period 1' (DOY 136–166); (b) 'Period 2' (DOY 167–196); (c) 'Period 3' (DOY 197–227), (d) 'Period 4' (DOY 228–269). The red and blue lines are 7-hour moving averages.

3.5 Net ecosystem exchange of CO_2

The CO_2 exchange dynamics at FLB3E during the growing season of 2022 were investigated employing the EC technique for continuous NEE measurements. Two temporal scales were analyzed: the diurnal time scale and the seasonal time scale. The diurnal patterns and magnitude of NEE were examined through NEE values binned by time of day and subsequently averaged. The seasonal scale was analyzed by observing daily average NEE values throughout the entire study period. This comprehensive examination of CO_2 exchange patterns at these various temporal scales offers valuable insights into the ecosystem's C dynamics and contributes to our understanding of its environmental significance.

3.5.1 Seasonal variation in the diurnal pattern of net ecosystem CO_2 exchange

Based on the NEE values binned by time of day for each period separately and subsequently averaged, Figure 3.6 shows that the ecosystem was a strong net sink of CO_2 from the atmosphere during the day and a weak source during the night during each of the four periods. The pattern of NEE exhibits a symmetrical diurnal cycle with peak uptake occurring at about 12:00 pm. The shift from source to sink occurred at about 7:00 am and returned to a source at about 7.00 pm, closely associated with sunrise and sunset times.

The diurnal patterns of NEE during the four different periods (period 1-4) representing vegetation growth stages exhibited similar shapes but demonstrated substantial variations in amplitude over the growing season of 2022, as illustrated in

Figure 3.6, Period 1, and period 4, representing the early and late stages of the growing season in 2022 at FLB3E, displayed a weak diurnal trend in NEE. In contrast, periods 2 and 3, characterized by relatively high soil moisture and warm temperatures compared to periods 1 and 4, exhibited a strong diurnal variation in NEE. Period 2 demonstrated the most pronounced diurnal NEE variation, with the ecosystem displaying a peak rate of net CO_2 uptake of approximately 9 μmol m^{-2} s^{-1} during daytime and CO_2 loss rates of approximately 5 μmol m^{-2} s^{-1} during nighttime. Notably, there was a fivefold increase in CO_2 uptake between period 1 and period 2.

The nighttime net ecosystem exchange (NEE) values observed between May and September displayed a range of approximately 1 to 6 μmol m^{-2} s^{-1}, indicating notable variations in respiration rates across the four periods (period 1-4). Similarly, daytime NEE values also exhibited significant fluctuations during this period, ranging from 0 to roughly 10 μmol m^{-2} s^{-1}, signifying varying degrees of net CO_2 uptake across the same four periods. It is evident that this pronounced daytime signal closely aligns with the available light for driving photosynthesis. During periods 2 and 3, the mean values of nighttime and early morning NEE showed increased variability when compared to periods 1 and 4. Furthermore, there was a slight variability in the timing of shifts between carbon sinks and sources within NEE throughout the different periods (1-4). These variations are likely attributable to changes in day length as the growing season progressed.

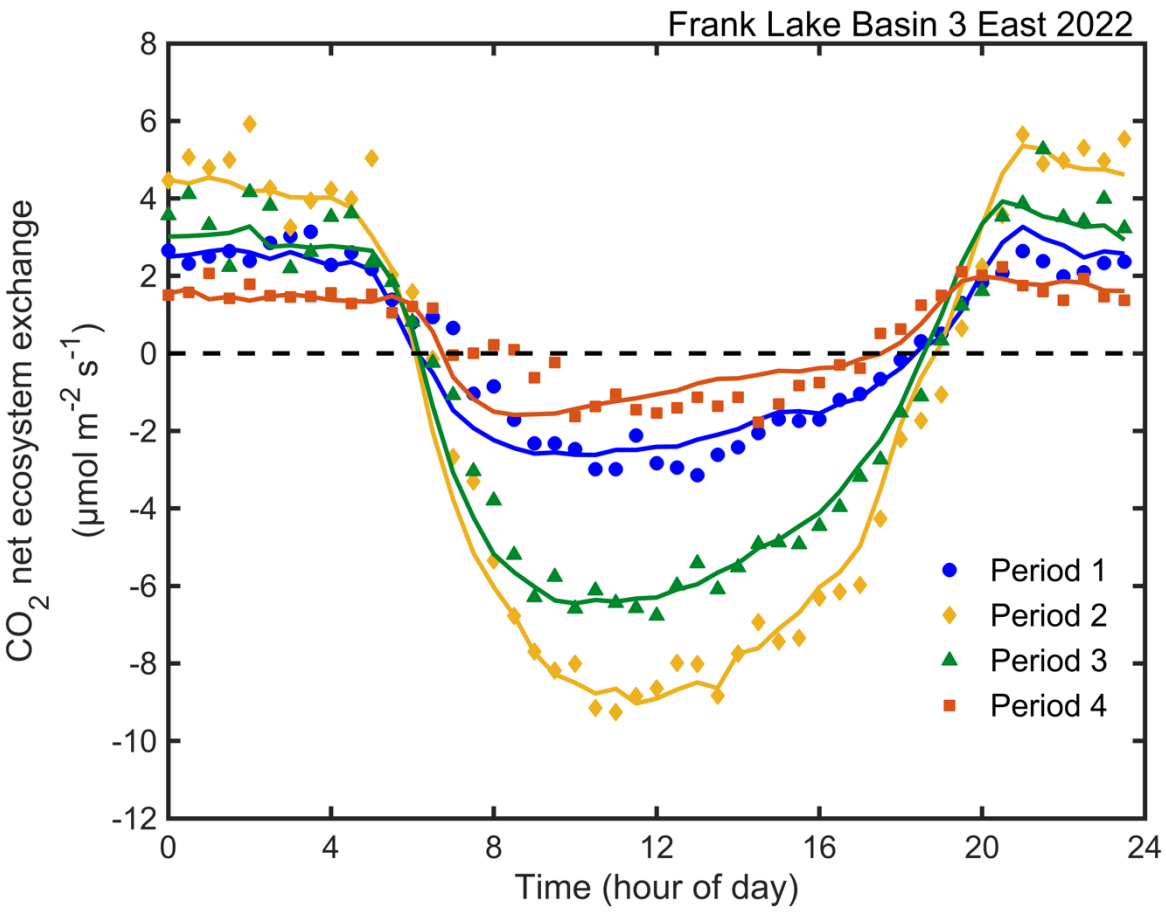

Figure 3.6: Comparison of seasonal variation in the mean diurnal pattern of net ecosystem CO_2 exchange (NEE) during the growing season of 2022 at Frank Lake Basin 3 East. The NEE values for each period were binned by time of day and averaged. Curves fitted are Michelas-Menten models. NEE = - $(A_{max}PPFD) / (A_{max}+PPFD) + (R_{10}Q_{10}^{(T-10)/10)})$

3.6 Seasonal variation in physiological capacity for photosynthesis and respiration

The ecosystem photosynthetic capacity (A_{max}) and respiratory capacity at 10^0C (R_{10}) were determined by fitting equation 7 to bin-averaged NEE data derived from the separate time periods (period 1-4) over the course of the growing season of 2022. The resulting parameters, A_{max} and R_{10} were plotted separately as functions of time (the day of year that fell in the center of each analyzed time period (Table 3.4, Figure 3.7). The coefficient of determination (r^2) for the nonlinear regression model equation was greater than 0.80 for all four periods, indicating a good fit. These figures provided valuable insights into the seasonal changes in the physiological and biochemical capacities of the ecosystem. Significant seasonal variations were observed for the ecosystem's photosynthetic capacity (A_{max}), photochemical efficiency (α), and respiratory capacity (R_{10}) at FLB3E, as indicated by the NEE model (Figure 3.7).

Both A_{max} and R_{10} initially (period 1) had low values, then reached peak values during period 2 and declined in the subsequent two periods (period 3 and 4). The A_{max} parameter ranged from 4.7 to 27.9 μmol m^{-2} s^{-1} across the analyzed four periods while R_{10} values ranged from 1.4 to 4.0 μmol m^{-2} s^{-1} based on the fitted NEE model (Figure 3.7). During all four periods, A_{max} values were greater than R_{10} values. The ecosystem reached the maximum A_{max} (27.9 μmol m^{-2} s^{-1}) and R_{10} (4.0 μmol m^{-2} s^{-1}) values, during the period 2 (~day 182). With an r^2 value of 0.98, data from period 2 was most closely fitted to the regression curve where photosynthesis showed the strongest response to light and respiration showed the strongest response to temperature compared to the other three seasonal periods. With a low r^2 value 0.80 when compared with other periods, period 4 showed the weakest relationship between photosynthesis and light

as well as between respiration and temperature. The photochemical efficiency (α), which represents the initial slope of the light-response curve, remained at 0.025 mol mol^{-1} during the growing season of 2022 except for the period 2, where it was 0.028 mol mol^{-1}. The Q_{10} parameter, representing the temperature sensitivity of respiration, consistently remained at 1.8 during all four periods (Table 3.4).

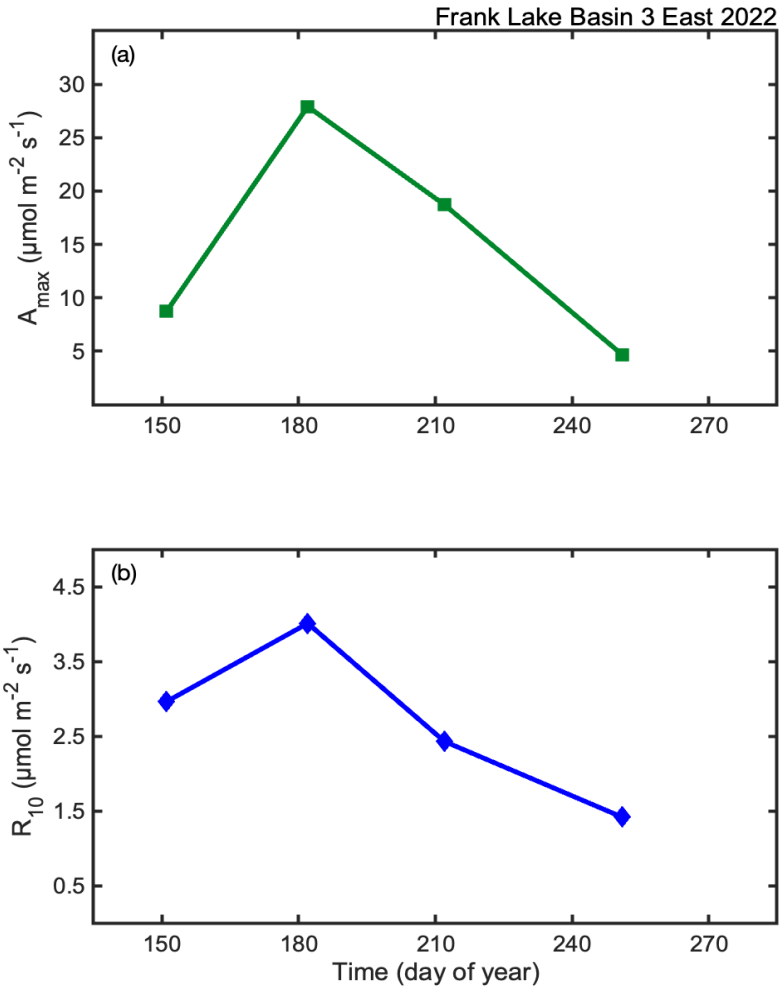

Figure 3.7: Seasonal variation in (a) calculated maximum ecosystem photosynthetic capacity (A_{max}) and, (b) ecosystem respiratory capacity normalized to 10^0C (R_{10})

Table 3.4: Comparison of non-linear regression parameters estimated using the Michelas-Menten (Equation 7) during the 2022 growing season. Models were parameterized using mean diurnal patterns (bin-averages by time of day, for approximately 15-day periods) of net ecosystem exchange (NEE), photosynthetically active photon flux density (PPFD) and air temperature from eddy covariance measurements at Frank Lake Basin 3 East, where r^2 is the coefficient of determination for each regression model.

Time period	α	Q_{10}	r^2
Period 1 (DOY 136–166)	0.025	1.8	0.93
Period 2 (DOY 167–196)	0.028	1.8	0.98
Period 3 (DOY 197–227)	0.025	1.8	0.97
Period 4 (DOY 228–269)	0.025	1.8	0.80

3.7 Seasonal variation of ecosystem CO_2 exchange processes

The GEP and TER values increased gradually from low values (2-3 g C m^{-2} day^{-1}) in mid-May (day 137) to reach peak values in July (10-12 g C m^{-2} day^{-1}) before declining to near minimum values (0.7-2.0 g C m^{-2} day^{-1}) at the end of September (day 273) (Figure 3.8). During period 1, GEP and TER exhibited a gradual increase from initial low levels. Net ecosystem exchange (NEE), representing the difference between GEP and TER, fluctuated between slightly negative and positive values, indicating alternating C sink and source dynamics. In period 2, both GEP and TER accelerated, although GEP displayed a higher rate. This resulted in a negative NEE, signifying the ecosystem's role as a C sink. The peak values of GEP, TER, and NEE occurred during this period, with a maximum daily NEE of approximately 5 g C m^{-2} day^{-1} observed around day 185. Subsequently, during period 3, both GEP and TER declined, while the NEE remained negative, indicating continued C uptake by the ecosystem. In period 4, GEP and TER decreased significantly, approaching near-zero levels by the end of the measurement period around day 273 where photosynthetic rates and respiratory rates became comparable during this phase, causing NEE to fluctuate near zero. Overall, TER closely tracked GEP, as indicated by the strong linear relationship between TER and GEP (r^2= 0.814, $p<0.01$). However, the maximum daily value of TER (day 196, 10.3 g C m^{-2} day^{-1}) did not coincide with the maximum daily value of GEP (12.7 g C m^{-2} day^{-1}, day 189), instead the maximum daily TER occurred with a lag of nearly one week after the maximum daily GEP. The seasonal pattern of NEE closely mirrored that of GEP, indicating that it was the driving component of seasonal variability of the CO_2 flux.

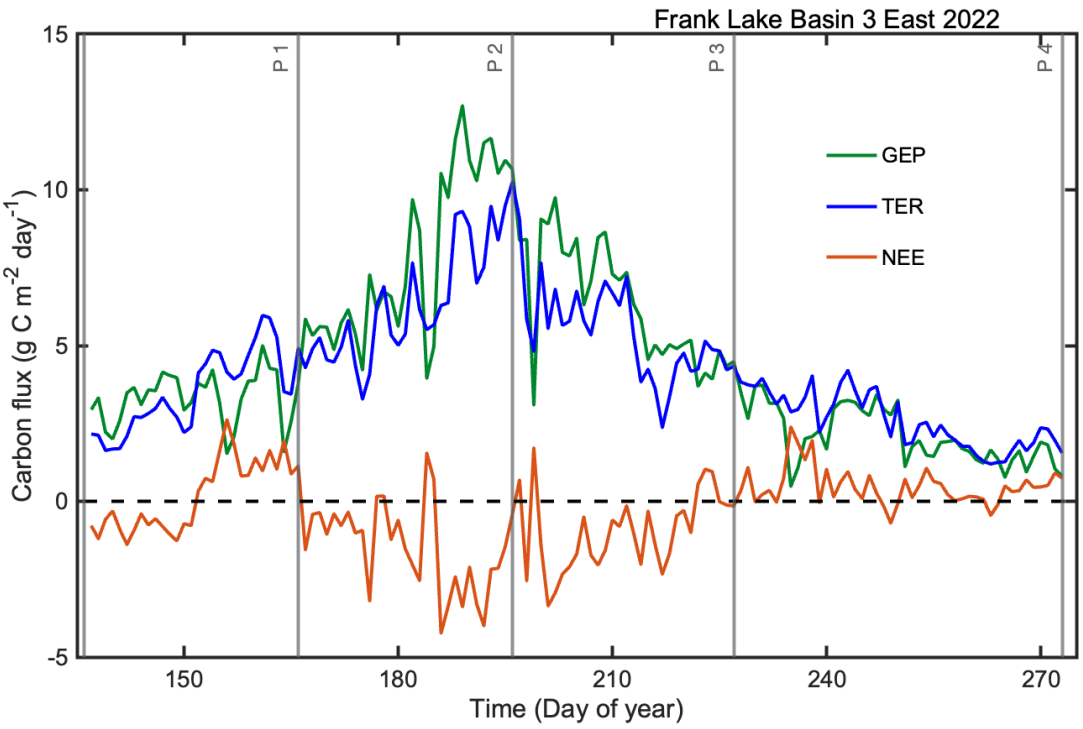

Figure 3.8: The daily integrated (a)gross ecosystem productivity (GEP), (b) total ecosystem respiration (TER), and (c) net ecosystem exchange (NEE) at Frank Lake Basin 3 East throughout the 2022 growing season. The vertical grey lines were used to separate the four phenological periods (P1-P4).

3.8 Controls on seasonal variation of ecosystem CO_2 exchange

As previously discussed in section 3.5.1, the primary environmental factors driving CO_2 exchanges include photosynthetically active radiation (PPFD), temperature, and soil moisture. Additionally, regional climate trends, such as drought events, exert a notable influence on the seasonal patterns of these key drivers. These climate trends represent a significant source of variability in year-to-year CO_2 exchange dynamics. Furthermore, synoptic-scale changes, characterized by dynamic weather conditions like precipitation, also play a role in shaping these surface-atmosphere exchanges. The following four paragraphs are mainly based on the trends shown in Figure 3.9.

At the onset of the growing season, GEP and TER exhibited low initial values (2-3 g C m^{-2} day^{-1}, day 137), associated with low temperatures (T_{air}~17^0C, T_{soil}~9^0C) and low PPFD (~15 mol m^{-2} day^{-1}), while soil water availably was moderate (0.4 m^3 m^{-3}). At the beginning of period 1 (day 136-152), both GEP and TER showed a gradual increase as temperature and PPFD started to increase. However, as the rate of increase in GEP was greater than that of TER, the ecosystem was a weak sink (-0.75 g C m^{-2} day^{-1}) for CO_2 from the atmosphere. The ecosystem shifted from a weak sink to a weak source on day 152, as TER started to increase associated with increasing temperatures. First bulrush green culms were observed around this day. A few large rain events also occurred between day 153-166 (second part of period 1), which affected the CO_2 budget in the bulrush marsh slightly. On day 157, a large rain event (14 mm) occurred which progressed to a couple of days. At the onset of this rain event, PPFD decreased to lowest recorded (~7 mol m^{-2} day^{-1}) and a decrease in GEP (~2.7 g C m^{-2} day^{-1}) was

observed with little to no effect on TER. Another large rain event occurred on day 164, where T_{air} declined by ~4° C and PPFD reached the lowest recorded during the study period (7 mol m^{-2} day^{-1}). With reduced PPFD and temperature, both GEP and TER declined, but TER was not reduced as much as GEP, similar to the response shown in the rain event on day 156 and the ecosystem remained a net weak source of CO_2 to the atmosphere (1.63 g C m^{-2} day^{-1}).

Period 2 was characterised by rapid growth of bulrushes. During the first portion of period 2 (~day 167-182), GEP was closely tracked by TER although GEP was slightly greater than TER, causing the ecosystem to be a weaker sink (-0.95 g C m^{-2} day^{-1}). Then, during the second portion of period 2 (~day 183-196), GEP took off and TER was low in comparison, which caused the ecosystem to be a significant net sink (-2.1 g C m^{-2} day^{-1}). Overall, the peak values of GEP, TER, and NEE occurred during this period, with a maximum daily NEE of approximately -4.2 g C m^{-2} day^{-1} (day 186). The peak PPFD (60 mol m^{-2} day^{-1}, day 176) was recorded during this period of rapid growth and photosynthesis. During this period, soil VWC and soil WP were high (0.47 m^3 m^{-3} and -10.8 kPa respectively) while T_{air} and T_{soil} were also high (14.6 and 13.6 ^{0}C respectively), although these were not the peak temperatures recorded during the study period. There was a strong correlation between TER and T_{soil} (r^2=0.71, $p<0.01$) as well as between TER and soil moisture (r^2=0.62, $p<0.01$) during this period, which was greater than all 3 other periods. It is noteworthy that even during the peak uptake period, a few positive NEE peaks can be observed. These are associated with rain events also with low PPFD and low temperatures, which decreased GEP dramatically, with less decrease in TER.

Despite maintaining relatively consistent values for PPFD to period 2 (Table 3.2 & 3.3), there was a steady decline in GEP during period 3. Notably, this period coincided with the maximum NDVI. The peak daily GEP (12.7 g C m-2 day-1) occurred around day 189 in period 2, whereas the peak NDVI (0.686) was observed later, around day 218 in period 3. This was due to the lag in the response of GEP to NDVI, although GEP approximately tracked NDVI. During the first part of period 3 (day 197-212), TER almost fluctuated at the same level while GEP started declining, and the ecosystem remained a sink. A sharp decline in soil moisture from about day 210 appears to be the main driver of this decline in GEP. During this period, the regression between Soil VWC and GEP was linear and significant (r^2=0.66, $p<0.05$). Then, during the second part of period 3 (day 213-227), TER started declining at a more rapid rate than GEP, so the ecosystem remained a sink. On about day 222, the ecosystem switched from a very weak sink of CO_2 to a weak source.

When soil moisture was exhausted in period 4, GEP continued its steady decline reaching low values, and as a result, this period represented the phase at which vegetation began to senesce. This reduction in GEP had little to no effect on TER observed in the marsh, making the ecosystem a source. By period 4, day length also decreased, which caused the average daily PPFD to decrease (32.87±8.83 mol m^{-2} day^{-1}). In addition, soil moisture levels declined and plateaued at about 0.3 m^3 m^{-3}. A small rain event (3 mm) occurred on day 252 but had little to no impact on recorded soil moisture levels. At this point, the capacity of the ecosystem for photosynthesis (A_{max}) and respiration (R_{10}) showed the lowest recorded from the 4 periods (~5 and ~1.5 µmol m^{-2} s^{-1} respectively, Figure 3.7).

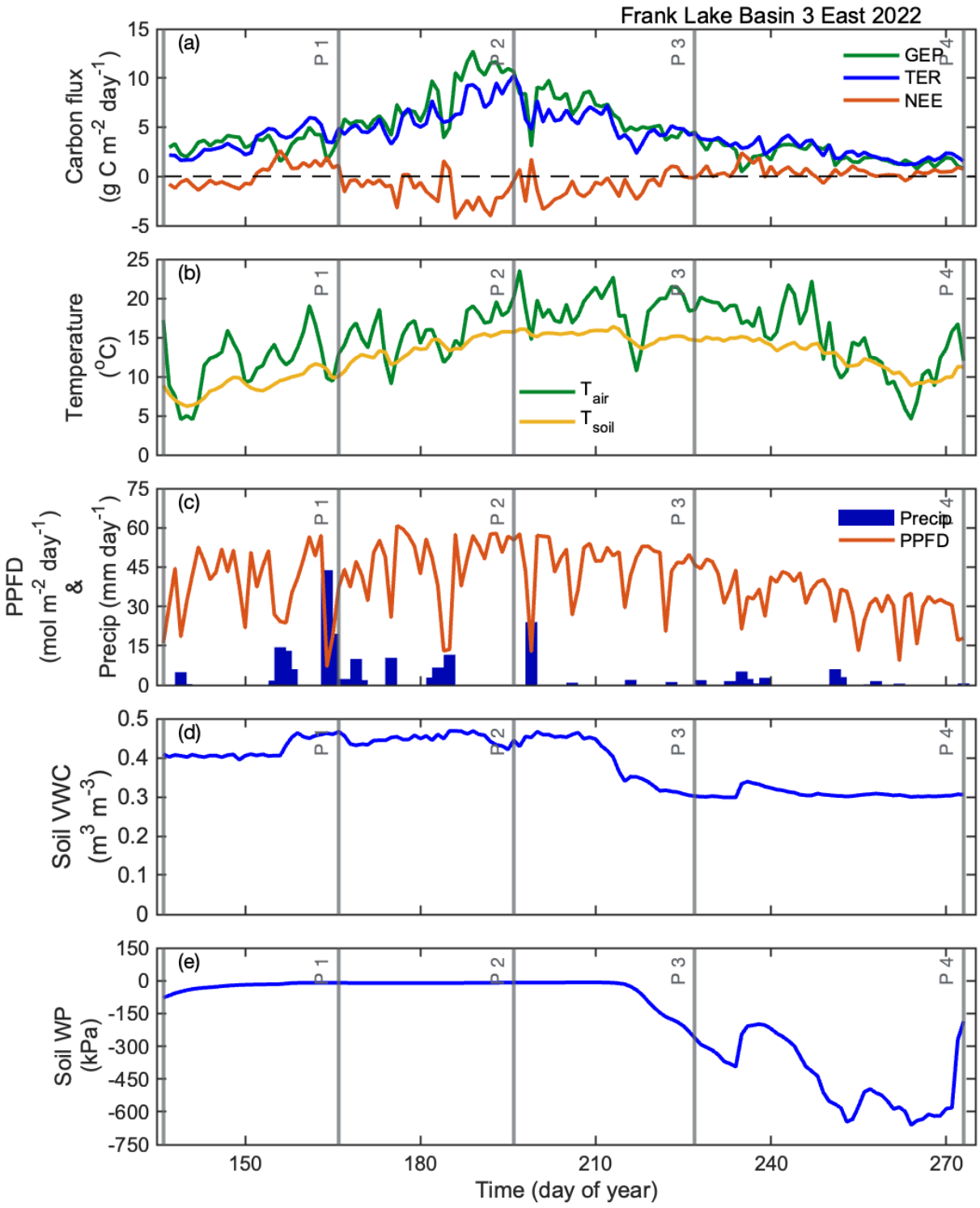

Figure 3.9: Mean daily pattern of CO_2 net ecosystem exchange (CO_2 NEE) measured at 4.5 m height above ground in Basin 3 East of Frank Lake, along with the mean daily patterns of associated environmental parameters. The vertical grey lines were used to separate the four phenological periods (P1-P4).

3.9 Diurnal variation of CH_4 net ecosystem exchange

The CH_4 NEE rates, as measured by the eddy covariance (EC) technique, exhibited a slight diurnal pattern with relatively lower values during the early morning and evening, and higher values during the early afternoon (Figure 3.10). This diurnal pattern of CH_4 net emission rates was most prominent during midday (10:00–17:00 h), and these patterns were found to be correlated with incoming solar radiation and friction velocity. However, it should be noted that the nighttime CH_4 NEE values displayed considerable fluctuations, partially due to a reduced number of data points resulting from friction velocity screening.

The CH_4 NEE provided an overview of the combined diurnal changes in its two component terms: storage flux and eddy flux. The storage flux, although generally low, exhibited an increase from nearly zero values during the period of approximately 12:00 to 20:00 hours. It maintained predominantly positive values throughout the night, from 18:00 to 06:00 hours. This relatively high storage of CH_4 can be attributed to the accumulation of CH_4 within the air space below the sonic anemometer during calm nighttime periods. The release of stored CH_4 into the atmosphere above the canopy occurred when sunrise initiated atmospheric mixing, causing the storage fluxes to become negative from approximately 07:00 to 12:00 hours. The mixing ratio of CH_4 increased progressively throughout the nocturnal period until sunrise.

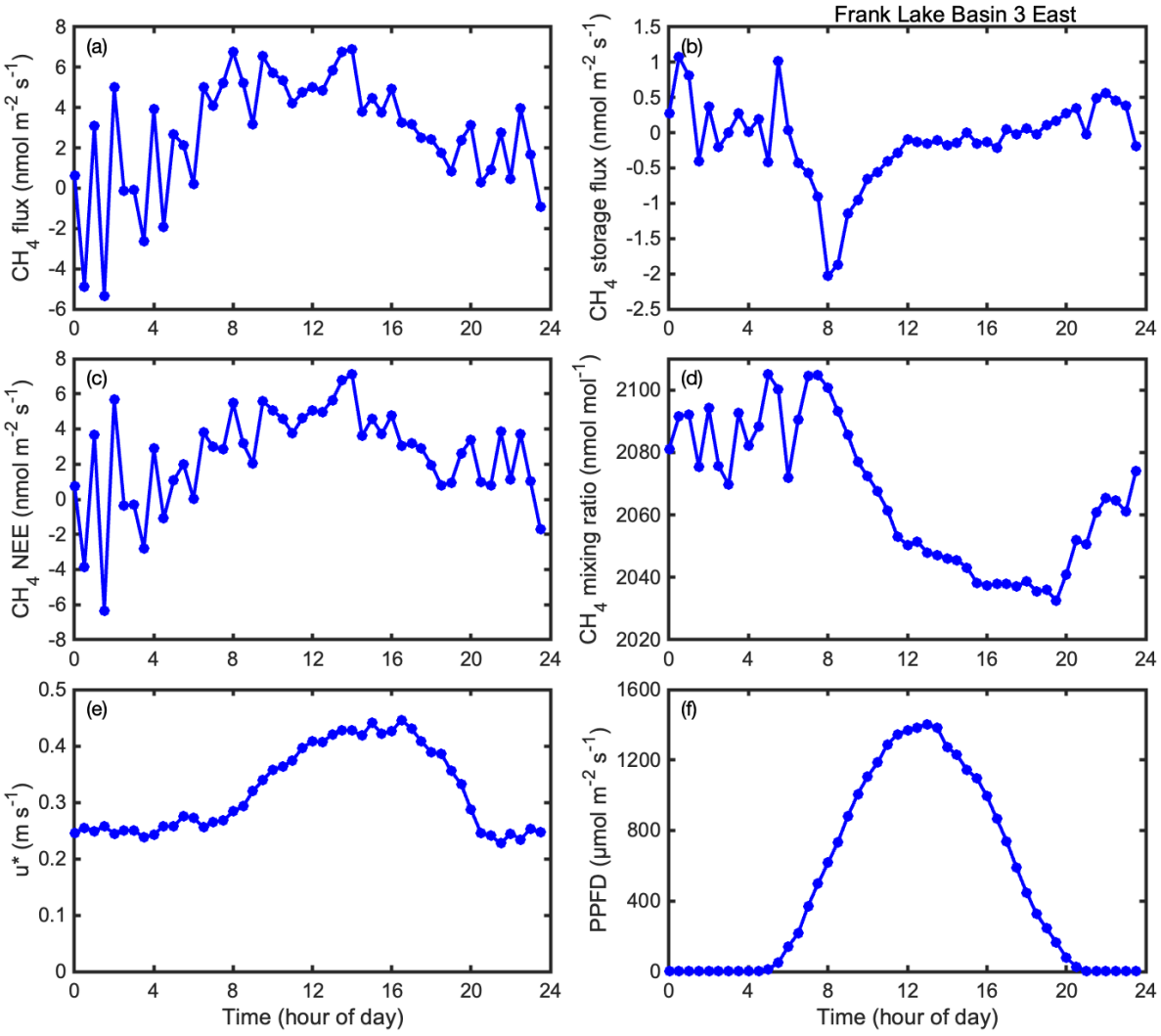

Figure 3.10: Mean diurnal pattern calculated for May–September 2022 of methane net ecosystem exchange (NEE) measured at 4.5 m height above ground in Basin 3 East of Frank Lake, Alberta. Negative values for the flux measurements represent net uptake (or storage) of methane by the ecosystem. PPFD is photosynthetically active photon flux density.

3.10 Seasonal variation of CH_4 net ecosystem exchange

When CH_4 net ecosystem exchange (CH_4 NEE) data were gap-filled and integrated into daily values, no clear seasonal trend of variation was observed (Figure 3.11). Throughout the growing season of 2022 at FLB3E, CH_4 net fluxes ranged from -3 to 10 mg C m^{-2} day^{-1}. Analyzing the half-hourly fluxes revealed relatively large variations in CH_4 emissions following the introduction of cattle on July 19th, 2022 (day 200, Figure 3.12). Peaks in CH_4 flux were not limited to specific times of the day but occurred at various times throughout the day. Aside from these occasional peaks, the CH_4 NEE half-hourly dataset exhibited minimal seasonal trends.

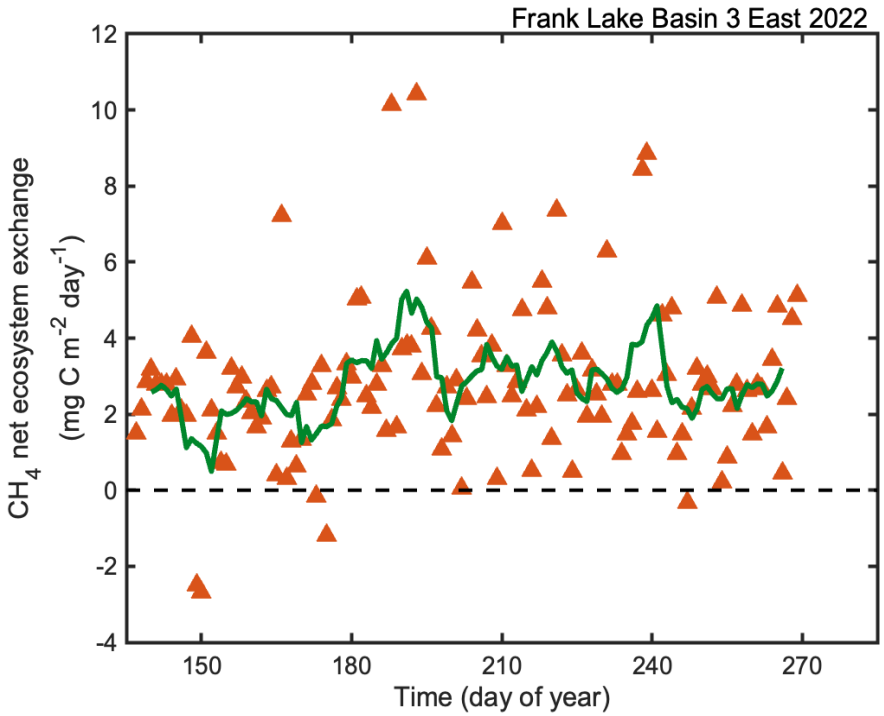

Figure 3.11: Seasonal pattern for May–September 2022 of CH_4 net ecosystem exchange (CH_4 NEE) measured at 4.5 m height above ground in Basin 3 East of Frank Lake, Alberta. Negative values for the flux measurements represent net uptake of methane by the ecosystem. The values are daily integrated values after gap filling 30 min data. The green line is the 7-day moving average.

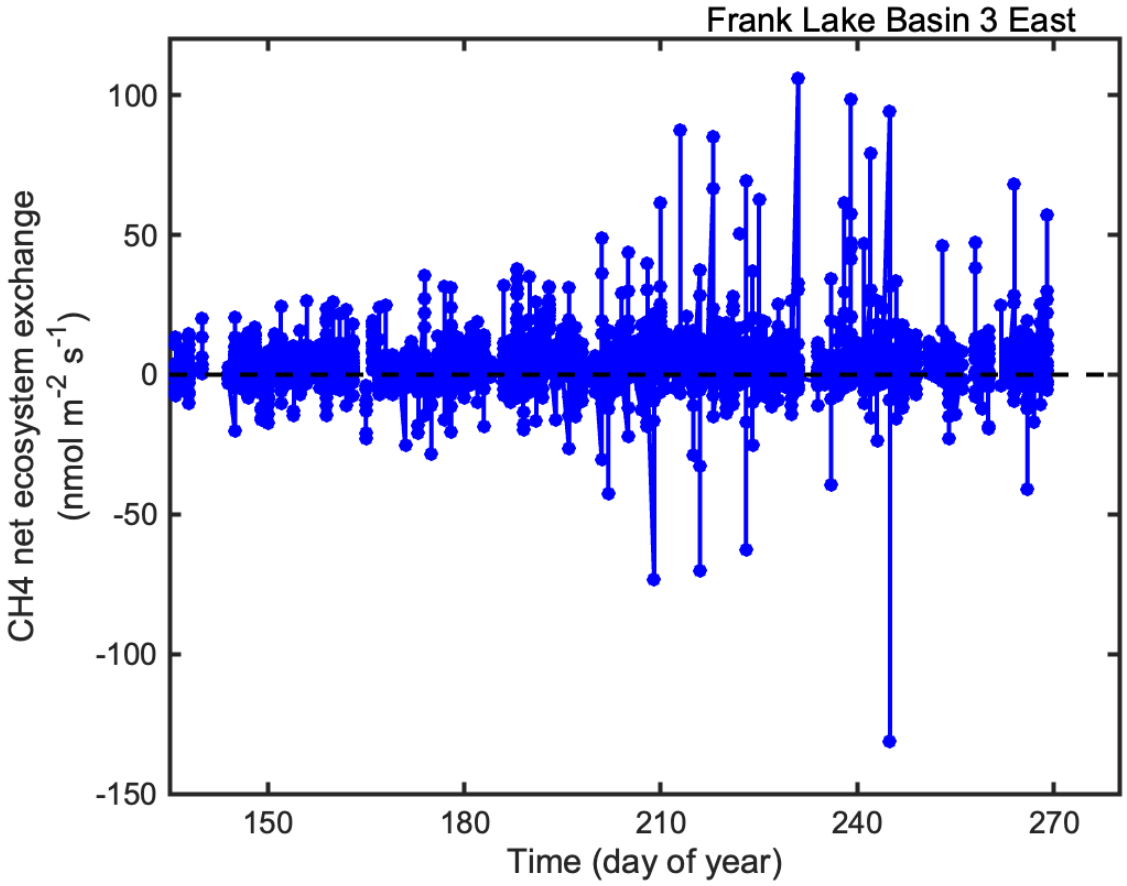

Figure 3.12: Seasonal pattern for May–September 2022 of CH_4 net ecosystem exchange (CH_4 NEE) measured at 4.5 m height above ground in Basin 3 East of Frank Lake, Alberta. Negative values for the flux measurements represent net uptake (or storage) of methane by the ecosystem. The values are non-gap-filled 30 min data.

3.11 Environmental and biotic controls on CH_4 exchange

Surprisingly, I observed that CH_4 NEE did not exhibit a significant correlation with any environmental or biotic parameters investigated in this study. Despite exploring various potential factors that could influence CH_4 NEE, such as meteorological variables and vegetation indices, no significant associations were found. This finding suggests that complex interactions may play a dominant role in shaping CH_4 NEE dynamics within the ecosystem under investigation.

3.12 Growing season carbon budget and global warming potentials

During the growing season of 2022, the ecosystem had total photosynthetic carbon uptake of 623 g C m^{-2} $season^{-1}$, while the total respiration was 575 g C m^{-2} $season^{-1}$, resulting in the wetland acting as a net CO_2 sink with a net uptake of 49 g C m^{-2} $season^{-1}$. Period 1 and 4 acted as sources for CO_2 (approximately 22 and 72 g C m^{-2} $period^{-1}$ respectively) and period 2 and 3 acted as net sinks for CO_2 (approximately -163 and -109 g C m^{-2} $period^{-1}$ respectively). FLB3E acted as small sources during all for periods for CH_4 with values ranging from ~4 to 7.5 g C m^{-2} $period^{-1}$ (Figure 3.13a). Methane net exchange (CH_4 NEE) for the growing season was calculated to be 6 g C m^{-2} $season^{-1}$ in CO_2-equivalents. This indicated that the ecosystem acted as a small positive source of CH_4 to the atmosphere during the May-September period. Considering both CO_2 and CH_4 emissions, the net carbon uptake of the ecosystem amounted to 43 g C m^{-2} $season^{-1}$ (Figure 3.13b). It is worth noting that the CH_4 emission rates, expressed in CO_2-equivalent units (CH_4 SGWP flux), offset only a small fraction (12.6%) of the CO_2 sequestration that occurred throughout the entire

growing season (seasonal total CH_4 flux: 6.13 g C m^{-2} (in CO_2-equivalents); seasonal total CO_2 flux: -48.7 g C m^{-2}).

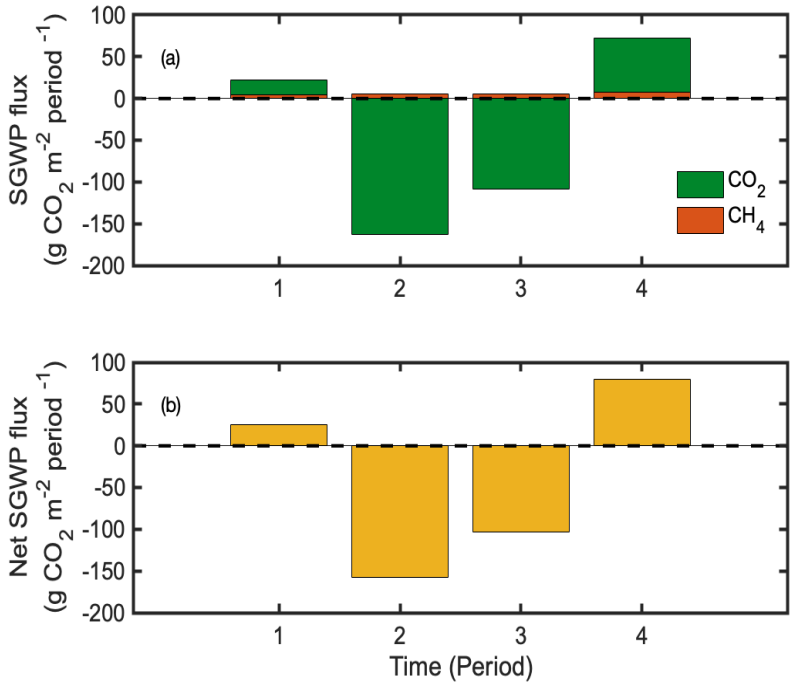

Figure 3.13: The seasonal variation in: (a) the sustained-flux global warming potential (SGWP) flux for CO_2 and CH_4, and (b) the net SGWP flux at Frank Lake Basin 3 East during the growing season of 2022. The net SGWP flux represents the sum of the CH_4 SGWP flux and CO_2 flux. The global warming potential fluxes were expressed in CO_2 equivalents and were calculated from the CH_4 flux data for a 100-year time horizon [where CH_4 equals 45 times the effect of CO_2 (on a mass basis)]. Time periods represent the following intervals: (1) 'Period 1' (DOY 136–166); (2) 'Period 2' (DOY 167–196); (3) 'Period 3' (DOY 197–227), (4) 'Period 4' (DOY 228–269).

CHAPTER 4: DISCUSSION

Prairie pothole wetlands serve as crucial C stores (Gleason *et al.*, 2009). However, conditions fostering organic C accumulation can also lead to the production of CH_4, a potent GHG with higher heat-trapping efficiency than CO_2 (Badiou *et al.*, 2011). These wetlands are among the most endangered ecosystems in North America, primarily due to historical and ongoing drainage linked to agricultural expansion (Badiou *et al.*, 2011). The full extent of the consequences of conversion of these wetlands remains unclear and requires further investigation. Understanding the behaviour of these GHGs from the restored prairie pothole wetlands will facilitate the understanding of the climate mitigation potential of this wetland through C sequestration. For Frank Lake in particular, the fluxes of both CO_2 and CH_4 are unclear, because it is a prairie pothole wetland restored using effluent water (Zhu *et al.,* 2019). The goal of this study was to determine whether the wetland at Frank Lake's Basin 3 acted as a source or sink for these two important greenhouse gases. The research also aimed to explore the factors influencing these fluxes, both environmental and biotic.

This study employed the eddy covariance technique to continuously measure the net ecosystem exchange (NEE) of CO_2 and CH_4 at FLB3E, a prairie wetland during the growing season of 2022. The growing season was marked by warmer temperatures and altered precipitation patterns compared to the long-term average, which influenced the phenological behaviour of the dominant macrophyte, bulrushes due to reduced water availability and no standing water at the wetland in April and May 2022. Divergent patterns in CO_2 and CH_4 fluxes emerged. Carbon dioxide displayed a seasonal trend, mirroring the vegetative growth cycle of bulrush, with net uptake

commencing in mid-May, peaking in mid-July, and declining by mid-September. In contrast, CH_4 fluxes exhibited no distinct seasonal patterns or correlations with plant phenology. Carbon dioxide fluxes, driven primarily by photosynthesis, revealed the wetland's role as a CO_2 sink (-49 g C m^{-2} s^{-1}) throughout the entire 2022 growing season. Methane fluxes, when integrated over the growing season and converted to CO_2-equivalents, remained exceptionally low at 6 g C m^{-2} s^{-1}, signifying a minor CH_4 source. This study conclusively demonstrated that the wetland functioned as a net sink (-43 g C m^{-2} s^{-1}) taking into account both CO_2 and CH_4 during the growing season, underscoring its crucial role in C sequestration and GHG mitigation.

To examine short-term temporal CO_2 flux patterns (diurnal and seasonal), I categorized the growing season into four distinct phenological stages based on the NDVI greenness index. These periods exhibited notable phenological variations and in most cases featured significantly distinct environmental conditions (Table 3.2 & 3.3), highlighting both environmental and phenological distinctions among these four stages. I observed a large diurnal trend of CO_2 net exchange, which resulted from the CO_2 uptake during photosynthesis and release during respiration (Figure 3.6). The daytime CO_2 uptake was driven by PPFD, which has been found as a dominant control of photosynthesis (Lafleur, 2009). During nighttime, when photosynthesis is inactive, the net ecosystem exchange (NEE) closely mirrored the magnitude and pattern of ecosystem respiration (TER). The amplitude of this diurnal trend was different for different phenological growth stages suggesting that there was a large seasonal variation of CO_2 exchange, and plant phenology and associated green LAI are major controls on these fluxes.

I observed a large seasonal variation in the daily-average net CO_2 exchange, which supports the seasonal pattern inferred from different diurnal trends observed during different phenologically and environmentally distinct phases. During the growing season, CO_2 uptake initiated in mid-May reached its peak in mid-July, and then gradually decreased starting from mid-August (Figure 3.2 & 3.8). This pattern indicated that the FLB3E ecosystem acted as a substantial CO_2 sink during the growth phases (periods 1, 2, and 3) when the emergent vegetation, mainly bulrush, was thriving, and it turned into a minor source during the senescence phase (period 4). As described by Knox *et al.*, (2015), this trend was marked by a rapid emergence, reaching peak growth, followed by a gradual decline in productivity as the vegetation entered the senescence stage. Research has consistently emphasized that plant phenology plays a pivotal role in shaping CO_2 exchange dynamics within wetland ecosystems, as demonstrated by previous studies (e.g., Bonneville *et al.,* 2008; Lund *et al.,* 2010).

Though evident that drought affects both soil respiration and photosynthesis in wetland plants (Alm *et al.*, 1999), it remained uncertain which of these effects held greater significance in the context of FLB3E during the year 2022. However, the seasonal fluctuations of CO_2 NEE closely mirrored those of GEP, emphasizing that GEP played a pivotal role in driving the seasonal variability of CO_2 flux during this relatively dry and warm year. There may have been multiple mechanisms at play to account for this outcome. Firstly, the rapid shoot growth of bulrushes could have efficiently absorbed a substantial amount of CO_2 while favourable conditions lasted (improved soil moisture, light exposure, and temperature). This was indicated by the five-fold increase (from periods 1 to 2) in CO_2 uptake observed in the diurnal trends of

CO_2 NEE (Figure 3.6). Additionally, high LE during period 2 indicated a high LAI and potentially increased stomatal conductance for CO_2 uptake. The highest CO_2 uptake occurred during this period (period 2), coinciding with a rapid increase in the NDVI, a commonly used proxy for LAI (Wang *et al.,* 2005). A higher LAI signifies a greater surface area covered by green leaves, thus facilitating enhanced light absorption and, consequently, an increased capacity for photosynthetic CO_2 uptake (Lafleur, 2009). Secondly, elevated nutrient content in FL, which is primarily attributed to the input of agro-industrial effluent, could have had a profound impact on plant growth and overall ecosystem C dynamics during the growing season of 2022 (Flanagan *et al.*, 2022). Finally, while soil respiration is typically strongly coupled to soil temperature, it's important to note that in certain ecosystems, microbial activity can be affected by soil moisture levels (Falge *et al.*, 2002). At FLB3E, it's possible that such a phenomenon occurred, leading to slightly lower respiration rates. Even though higher soil temperatures generally favour respiration, the presence of low soil moisture content may have caused a reduction in microbial activity, potentially due to microbe dormancy. This was contrary to our expectation of increased respiration with higher temperatures.

Despite experiencing unusually dry and warm conditions, FLB3E continued to exhibit its capacity as a net CO_2 sink during the growing season of 2022. A comprehensive study conducted by Badiou *et al.,* (2011) that involved 62 wetlands in the prairie pothole region of Canada, assessed C sequestration rates by analyzing changes in soil organic carbon (SOC) and CH_4 fluxes via chamber measurements. When considering only CO_2 exchange, Badiou *et al.,* (2011) reported an average C sequestration rate of -270 g C m^{-2} $year^{-1}$. Moreover, Tangen and Bansal, (2020) in another survey of 549

wetlands in the PPR showed an average C sequestration rate of -100 g C m^{-2} $year^{-1}$. In contrast, a much lower C sequestration rate (-49 g C m^{-2} $season^{-1}$) was observed at the FLB3E wetland during the growing season of 2022. However, it is noteworthy that the important ecosystem service of C sequestration could still occur in prairie pothole wetlands even in unusual climatic conditions. Further multiyear research is required in similar climate conditions in prairie pothole wetlands to see how this sink/source status shifts in years with more favourable conditions for plant growth.

Lack of standing water and low soil moisture availability in the dry year of 2022 led to a delayed emergence and early senescence of bulrushes, shortening the growing season to approximately 100 days. In a more typical year at Frank Lake, the growing season extends to around 150 days (Figure 3.2). A longer growing season indicates a prolonged period favourable for C assimilation (Randerson *et al.*, 1999). In years with more favourable environmental conditions closer to the climatic average, FL has the potential to function as a more robust CO_2 sink than it did in 2022. However, potential shifts in photosynthetic and microbial activities may diminish or even reverse the advantages of an extended growing season for C sequestration. The disproportionate responses of photosynthesis and respiration to moisture anomalies deserve more attention because even a small change in these two large C fluxes may translate to considerable changes in the magnitude and direction of CO_2 sequestration. Therefore, conducting long-term studies is imperative to gain a comprehensive understanding of the wetland's C sequestration dynamics under varying climatic conditions.

A subtle diurnal pattern became evident in CH_4 net exchange when analyzing the data spanning the entire growing season, and this pattern was closely linked to the friction

velocity, as illustrated in Figure 3.10. Specifically, during nights with low friction velocity (calm conditions), CH_4 tended to accumulate in the canopy airspace, remaining undetected by the EC instruments. However, as atmospheric turbulent mixing resumed during the day, the previously stored CH_4 was flushed out and captured by the EC system. As a result, variations in CH_4 fluxes between daytime and nighttime formed a diurnal cycle, driven by changes in friction velocity. To ensure the reliability of CH_4 flux measurements using the EC technique, I carefully screened the CH_4 NEE dataset, excluding data from periods with insufficient turbulence. It's important to note that even though I implemented this screening process, my analysis didn't entirely eliminate the influence of diurnal turbulence fluctuations on CH_4 NEE. Moreover, certain prior studies, such as one conducted in a northern peatland, noted marked diurnal variations in CH_4 net flux during the peak of the growing season (Long *et al.*, 2010). Conversely, other studies, like the one in a boreal, nutrient-poor fen in Finland, found no significant diurnal variation in CH_4 net flux (Rinne *et al.*, 2007).

The diurnal cycle of CH_4 at FLB3E may be influenced by other mechanisms beyond friction velocity, particularly due to the presence of dense bulrush vegetation. Additional factors could include diurnal fluctuations in convective flow through wetland plants (Whiting and Chanton, 1996), variations in stomatal conductance within plants (Garnet *et al.*, 2005), and the transpiration of water vapour containing dissolved CH_4 (Nesbit *et al.*, 2009). In future research, it is advisable to explore the role of plant-mediated transport of CH_4 at Frank Lake which could provide valuable insights into the wetland's CH_4 dynamics.

I extended the analysis to investigate short-term temporal patterns in CH_4 fluxes, following a similar period-wise approach as used for CO_2 fluxes (not presented here). However, this investigation did not reveal any distinct differences in CH_4 fluxes across these phenologically different periods, indicating an absence of a link between plant phenology and CH_4 fluxes as well as the absence of a seasonal trend in CH_4 fluxes. Similarly, when examining the daily-average values of CH_4 net ecosystem exchange, no significant seasonal patterns in CH_4 exchange were evident (Figure 3.11). The CH_4 net fluxes fluctuated within a narrow range (-4 to 12 mg C m^{-2} day^{-1}), in contrast to findings from a northern Canadian peatland study, where a distinct and substantial seasonal variation in daily average CH_4 net flux was observed. In that study, CH_4 values transitioned from near-zero levels to a peak of approximately 83 g C m^{-2} day^{-1} (Long *et al.*, 2010).

Cattle were introduced to Frank Lake for grazing on July 19th, 2022 (day 200), and their immediate impact on CO_2 and CH_4 fluxes wasn't evident when looking at daily-integrated patterns. However, a significant increase in variability became noticeable within the half-hour CH_4 fluxes, coinciding with their introduction during the peak growth period (period 3) and persisting throughout the rest of the observation period (Figure 3.12). Baldocchi *et al.*, (2012) stated that the presence of cattle within the flux footprint notably impacts CH_4 fluxes with a relatively minor influence on CO_2 fluxes. This influence of cattle on CH_4 emissions in wetlands is attributed to enteric fermentation, a natural process in ruminants like cattle, which leads to CH_4 production through the bacterial breakdown of consumed feed (Naqvi and Sejian, 2011). The cattle were intermittently present near the tower and occasionally approached the tower for activities like body rubbing. As a result, they had only a

minor influence on the wetland's C budget. This suggests that cattle emissions are likely not a major factor affecting the C budget at Frank Lake, indicating that the wetland's overall C dynamics are more strongly influenced by other factors, such as climate conditions and vegetation characteristics.

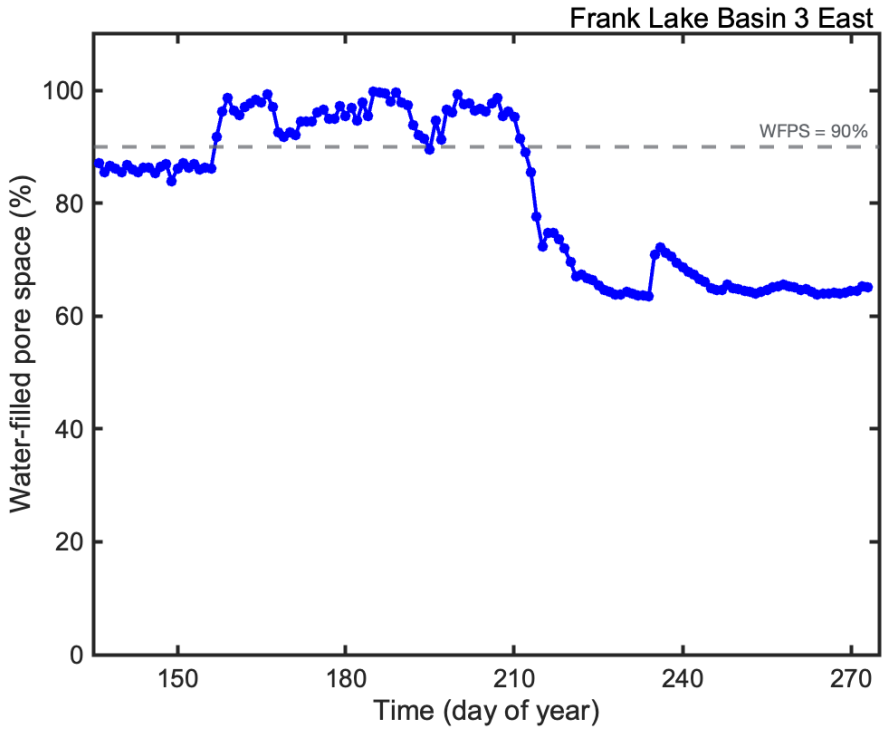

Figure 4.1: Water-filled pore space (WFPS, %) calculated using the Soil VWC measured at 15 cm depth. The equation used for the calculation of WFPS was WFPS = Soil VWC/1 - (BD/PD). Bulk density (BD) was assumed to be 1.4 g cm^{-3} and particle density (PD) was assumed to be 2.65 g cm^{-3}. The grey dashed line represents WFPS = 90%

Throughout the growing season of 2022 at FLB3E, CH_4 fluxes remained exceptionally low (6 g C m^{-2} $season^{-1}$ in CO_2-equivalents). A model developed by Bansal *et al.*, (2023) for prairie pothole wetlands, suggests that CH_4 emissions sharply decrease when soil moisture drops below 90% (measured as water-filled pore space). At FLB3E the soil

moisture levels were low and was typically below 0.45 m^3 m^{-3} (Figure 3.4c). When the water filled pore space (WFPS) was calculated with Soil VWC measurements made at 15 cm depth (Figure 4.1), it remained below 90% for most of the growing season. This could explain the extremely low CH_4 emissions at FLB3E. Despite indications of a non-linear increase in CH_4 emissions with rising temperatures and significant contributions from emergent vegetation (as reflected in positive NDVI values), the primary factor influencing CH_4 emissions, according to the model by Bansal *et al.*, (2023), was soil moisture. Similarly, at FLB3E, although favourable temperatures and abundant bulrush vegetation were present for at least a part of the growing season, CH_4 emissions remained low due to limited standing water and generally insufficient soil moisture.

It's possible that while CH_4 production did occur, oxic soil conditions likely led to CH_4 oxidation, contributing to the observed low CH_4 fluxes. Previous studies have shown that the presence of a thin oxic layer within an otherwise anaerobic environment can trigger CH_4 oxidation, resulting in a significant reduction in CH_4 emissions, potentially up to 90% (Roslev and King, 1996). Additionally, the hydroperiod, or the duration of standing water, could also influence CH_4 emissions, as highlighted by Bansal *et al.,* (2023). During the growing season of 2022, there was very little standing water, lasting approximately 10 days (Figure 3.4d), and, as a result, the topsoil layers (above 15 cm depth) remained unsaturated for most of the growing season. This contrasts with the typical hydroperiod of 120-140 days in prairie pothole wetlands (Bansal *et al.,* 2023), potentially explaining the low CH_4 emissions observed at FLB3E.

FLB3E, with its 40-hectare size, qualifies as a large wetland according to Bansal *et al.*, (2023). However, when considering the broader criteria for large wetlands, which include features like higher salinity, sparse vegetation, and lower soil C content, FLB3E doesn't meet the large wetland definition provided by Bansal *et al.*, (2023). FLB3E has low salinity, abundant macrophyte vegetation, and higher soil C content (Zhu *et al.*, 2019; Flanagan *et al.*, 2022). I observed substantial growth of bulrushes at FLB3E even in the relatively dry conditions of 2022. In a typical year with more bulrush vegetation and standing water, it's expected that the wetland would release higher CH_4 emissions. This leads to the classification of FLB3E as a medium-sized wetland, referred to as the 'Goldilocks' category by Bansal *et al.*, (2023), which has the highest potential for CH_4 production and emission.

The growing season C budget calculated for the FLB3E indicated that the wetland acted as a net C sink (-43 g C m^{-2} $season^{-1}$) considering both CO_2 and CH_4 fluxes. Prior research underscores the importance of CH_4 fluxes in prairie pothole wetland C budgets, suggesting that C loss through CH_4 emissions may not be compensated by net CO_2 uptake (Badiou *et al.*, 2011). However, the observed net CH_4 emission rates at FLB3E in 2022 were considerably lower than the rates of net CO_2 sequestration. Consequently, CH_4 emission rates, expressed as CO_2-equivalent units (CH_4 SGWP flux), offset only a small fraction (12.6%) of the CO_2 sequestration over the entire growing season.

The survey of PPR wetlands conducted by Badiou *et al.*, (2011), emphasized the importance of CH_4 fluxes within prairie pothole wetland C budgets, highlighting that the C loss through CH_4 emissions might offset a larger portion of net CO_2 uptake.

Badiou *et al.,* (2011) recorded a CO_2 uptake rate of -270 g C m^{-2} $year^{-1}$ and a CH_4 emission rate of 20 g C-CH_4 m^{-2} $year^{-1}$ for wetlands in prairie pothole region of Canada. Badiou *et al.*, (2011) used a global warming potential (GWP) of 25 (mass basis) for a 100-year time horizon to convert CH_4 to CO_2-equivalents described in Forster *et al.*, (2007) and calculated the CH_4 emission to be 181.8 g C m^{-2} $year^{-1}$. Therefore, when accounting for both CO_2 and CH_4, Badiou *et al.*, (2011) found that the net C sequestration rate was reduced from -270 to -88.2 g C m^{-2} $year^{-1}$ (-270 +181.8 g C m^{-2} $year^{-1}$). The net C sink strength at FLB3E (-43 g C m^{-2} $season^{-1}$) was approximately half of the net C sequestration value (considering CO_2 and CH_4 fluxes) recorded in Badiou *et al.*, (2011). This still represents a significant C sink at FLB3E, considering the relatively dry and warm conditions that prevailed during the study. The results from this study suggest that prairie pothole wetlands, such as Frank Lake, can act as important C sinks, even in the face of dry and warm conditions, as observed in the year 2022.

However, it's noteworthy that Badiou *et al.,* (2011) utilized a global warming potential (GWP) for pulse emissions of CH_4 as described by Forster *et al.*, (2007). Recognizing that these GHGs persist in the environment, in my study I employed a sustained global warming potential (SGWP) of 45 (on a mass basis) over a 100-year time horizon consistent with Neubauer & Megonigal (2015). I adopted the same SGWP conversion factor (45), to convert CH_4 fluxes in Badiou *et al.*, (2011) to CO_2-equivalents and it was calculated to be 327.3 g C m^{-2} $year^{-1}$. Subsequently, when factoring in both CO_2 and CH_4, the net C sequestration rate underwent a notable shift, reducing from -270 to 57.3 g C m^{-2} $year^{-1}$ (-270 + 327.3 g C m^{-2} $year^{-1}$). This underscores the pivotal role of the chosen GWP factor when converting CH_4 to CO_2-equivalents and highlights that

the ecosystem's status, whether a C sink or source, is contingent on this choice. Consequently, careful consideration of the GWP factor is essential in C accounting and climate change assessments.

My study, which offers a comprehensive analysis of C dynamics during a growing season in a prairie pothole wetland using the eddy covariance technique, contributes significantly to the existing literature. This is particularly important because EC studies in the prairie pothole region (PPR) are limited, with previous research relying mostly on measurement of stores of SOC for determining C sequestration rates and using chamber measurements for GHG assessments (Badiou *et al.*, 2011; Tangen and Bansal, 2020). Nonetheless, further research is needed, specifically including the context of wintertime at prairie wetlands like Frank Lake, since photosynthesis ceases in the winter, yet respiration continues, albeit at a reduced rate (Lafleur, 2009). Moreover, although I focussed only on vertical C fluxes during my study, future research endeavours that encompass both lateral and vertical C fluxes are crucial to obtain a more holistic perspective of C cycling within wetland ecosystems (Chu *et al.,* 2015). Such studies will advance our knowledge of C dynamics and contribute to more accurate assessments of C sequestration and GHG emissions in these critical ecosystems.

CHAPTER 5: CONCLUSIONS

In this study, I investigated the CO_2 and CH_4 fluxes in Frank Lake, a prairie pothole wetland, during the growing season of 2022. Utilizing the EC technique, I continuously monitored these fluxes in a growing season characterized by warmer temperatures and altered precipitation patterns compared to the long-term average. My findings provide valuable insights into the dynamics of GHG exchange in wetlands under changing environmental conditions. Despite the warmer and relatively dry weather in 2022, Frank Lake proved to be a important sink for atmospheric CO_2 throughout the study period, taking into consideration both CO_2 and CH_4. This observation underscores the remarkable capacity of this prairie pothole wetland to sequester CO_2 from the atmosphere, even under conditions typically associated with reduced C uptake. It highlights the vital ecosystem service of CO_2 sequestration, emphasizing the potential for wetlands to help mitigate climate change, even in the face of warming and altered precipitation patterns.

Throughout the growing season, my analyses revealed that a general lack of standing water and reduced soil moisture availability emerged as the dominant factor influencing C cycling, surpassing the influence of soil temperature and light availability. This underscores the critical role of hydrological conditions in governing C dynamics within wetland ecosystems. Furthermore, I observed that different C fluxes responded unequally to environmental and biotic factors, implying that the FLB3E C budget may exhibit substantial variation from year to year. Considering these findings, future research in wetland ecosystems should emphasize the intricate interplay of various C processes in response to changing environmental conditions.

Understanding these dynamics is not only essential for accurately assessing the C balance of wetlands but also for predicting their role in the broader context of global C cycling and climate change mitigation. Wetlands, like Frank Lake, are not only valuable biodiversity habitats but also play a crucial role as nature-based solutions in our efforts to combat climate change. In conclusion, my study contributes to a deeper understanding of the resilience and significance of wetland ecosystems in sequestering C, offering hope that they can continue to provide this vital ecosystem service even as climate conditions evolve.

REFERENCES

Alm, J., Schulman, L., Walden, J., Nykänen, H., Martikainen, P. J. & Silvola, J. (1999). Carbon balance of a boreal bog during a year with an exceptionally dry summer. *Ecology*, *80(1)*, 161-174. https://doi.org/10.1890/0012-9658(1999)080[0161:CBOABB]2.0.CO;2

Badiou, P., McDougal, R., Pennock, D. & Clark, B. (2011). Greenhouse gas emissions and carbon sequestration potential in restored wetlands of the Canadian prairie pothole region. *Wetlands Ecology and Management*, *19*, 237-256.

Baldocchi, D. (2003). Assessing the eddy covariance technique for evaluating carbon dioxide exchange rates of ecosystems: past, present and future. *Global change biology, 9(4)*, 479-492. https://doi.org/10.1046/j.1365-2486.2003.00629.x

Baldocchi, D. (2014). Measuring fluxes of trace gases and energy between ecosystems and the atmosphere–the state and future of the eddy covariance method. *Global Change Biology*, *20(12)*, 3600-3609. https://doi.org/10.1111/gcb.12649

Baldocchi, D., Detto, M., Sonnentag, O., Verfaillie, J., The, Y. A., Silver, W. & Kelly, N. M. (2012). The challenges of measuring methane fluxes and concentrations over a peatland pasture. *Agricultural and Forest Meteorology*, *153*, 177-187. https://doi.org/10.1016/j.agrformet.2011.04.013

Bansal, S., Post van der Burg, M., Fern, R. R., Jones, J. W., Lo, R., McKenna, O. P. & Gleason, R. A. (2023). Large increases in methane emissions expected from North America's largest wetland complex. *Science Advances*, *9(9)*, eade1112. https://doi.org/10.1126/sciadv.ade1112

Barr, A. G., Morgenstern, K., Black, T. A., McCaughey, J. H. & Nesic, Z. (2006). Surface energy balance closure by the eddy-covariance method above three boreal forest stands and implications for the measurement of the CO_2 flux. *Agricultural and Forest Meteorology*, *140(1-4)*, 322-337. https://doi.org/10.1016/j.agrformet.2006.08.007

Bonneville, M. C., Strachan, I. B., Humphreys, E. R. & Roulet, N. T. (2008). Net ecosystem CO_2 exchange in a temperate cattail marsh in relation to biophysical properties. *Agricultural and Forest Meteorology*, *148(1)*, 69-81. https://doi.org/10.1016/j.agrformet.2007.09.004

Brix, H. (1993). Macrophyte-mediated oxygen transfer in wetlands: transport mechanisms and rates. *Constructed wetlands for water quality improvement,* 391-398.

Bubier, J. L. & Moore, T. R. (1994). An ecological perspective on methane emissions from northern wetlands. *Trends in Ecology & Evolution*, *9(12)*, 460-464. https://doi.org/10.1016/0169-5347(94)90309-3

Chamberlain, S. D., Hemes, K. S., Eichelmann, E., Szutu, D. J., Verfaillie, J. G. & Baldocchi, D. (2020). Effect of drought-induced salinization on wetland methane emissions, gross ecosystem productivity, and their interactions. *Ecosystems*, *23(3)*, 675-688.

Chapin, F. S., Woodwell, G. M., Randerson, J. T., Rastetter, E. B., Lovett, G. M., Baldocchi, D. & Schulze, E. D. (2006). Reconciling carbon-cycle concepts, terminology, and methods. *Ecosystems*, *9(7)*, 1041-1050.

Chen, H., Xu, X., Fang, C., Li, B. & Nie, M. (2021). Differences in the temperature dependence of wetland CO_2 and CH_4 emissions vary with water table depth. *Nature Climate Change*, *11(9)*, 766-771.

Chu, H, Gottgens, J. F., Chen, J., Sun, G., Desai, A. R., Ouyang, Z. & Czajkowski, K. (2015). Climatic variability, hydrologic anomaly, and methane emission can turn productive freshwater marshes into net carbon sources. *Global Change Biology*, *21(3)*, 1165-1181. https://doi.org/10.1111/gcb.12760

Cohen-Shacham, E., Walters, G., Janzen, C. & Maginnis, S. (2016). Nature-based solutions to address global societal challenges. *IUCN: Gland, Switzerland*, *97*, 2016-2036. https://doi.org/10.2305/IUCN.CH.2016.13.en

Covey, K. R. & Megonigal, J. P. (2019). Methane production and emissions in trees and forests. *New Phytologist*, *222(1)*, 35-51. https://doi.org/10.1111/nph.15624

Falge, E., Baldocchi, D., Tenhunen, J., Aubinet, M., Bakwin, P., Berbigier, P. & Wofsy, S. (2002). Seasonality of ecosystem respiration and gross primary production as derived from FLUXNET measurements. *Agricultural and Forest Meteorology*, *113(1-4)*, 53-74. https://doi.org/10.1016/S0168-1923(02)00102-8

Flanagan, L. B., Henry, K. J., Telfer, M. D., Zimmerman, O. R., Soued, C. & Bogard, M. J. (2022). Small contribution of *Schoenoplectus acutus* (emergent macrophyte) to nitrogen removal from wastewater effluent input to a restored prairie wetland complex. *Wetlands*, *42(8)*, 105.

Forster, P., Ramaswamy, V., Artaxo, P., Berntsen, T., Betts, R., Fahey, D.W., Haywood, J., Lean, J., Lowe, D.C., Myhre, G. & Nganga, J. (2007). Changes in atmospheric constituents and in radiative forcing. *Climate Change 2007. The Physical Science Basis.*

Garnet, K. N., Megonigal, J. P., Litchfield, C. & Taylor Jr, G. E. (2005). Physiological control of leaf methane emission from wetland plants. *Aquatic Botany*, *81(2)*, 141-155. https://doi.org/10.1016/j.aquabot.2004.10.003

Gleason, R. A., Tangen, B. A., Browne, B. A. & Euliss Jr, N. H. (2009). Greenhouse gas flux from cropland and restored wetlands in the Prairie Pothole Region. *Soil Biology and Biochemistry*, *41(12)*, 2501-2507. https://doi.org/10.1016/j.soilbio.2009.09.008

Gomez-Casanovas, N., DeLucia, N. J., DeLucia, E. H., Blanc-Betes, E., Boughton, E. H., Sparks, J. & Bernacchi, C. J. (2020). Seasonal controls of CO_2 and CH_4 dynamics in a temporarily flooded subtropical wetland. *Journal of Geophysical Research: Biogeosciences*, *125(3)*, e2019JG005257. https://doi.org/10.1029/2019JG005257

Grünfeld, S. & Brix, H. (1999). Methanogenesis and methane emissions: effects of water table, substrate type and presence of Phragmites australis. *Aquatic Botany*, *64*, 63-75. https://doi.org/10.1016/S0304-3770(99)00010-8

Helfter, C., Gondwe, M., Murray-Hudson, M., Makati, A. & Skiba, U. (2022). From sink to source: high inter-annual variability in the carbon budget of a Southern African wetland. *Philosophical Transactions of the Royal Society A*, *380(2215)*, 20210148. https://doi.org/10.1098/rsta.2021.0148

Hemes, K. S., Chamberlain, S. D., Eichelmann, E., Knox, S. H. & Baldocchi, D. (2018). A biogeochemical compromise: The high methane cost of sequestering carbon in restored wetlands. *Geophysical Research Letters*, *45(12)*, 6081-6091. https://doi.org/10.1029/2018GL077747

Herbst, M., Friborg, T., Ringgaard, R. & Soegaard, H. (2011). Interpreting the variations in atmospheric methane fluxes observed above a restored wetland. *Agricultural and Forest Meteorology*, *151(7)*, 841-853. https://doi.org/10.1016/j.agrformet.2011.02.002

Joabsson, A. & Christensen, T. R. (2001). Methane emissions from wetlands and their relationship with vascular plants: an Arctic example. *Global Change Biology*, *7(8)*, 919-932. https://doi.org/10.1046/j.1354-1013.2001.00044.x

Joabsson, A., Christensen, T. R. & Wallén, B. (1999). Vascular plant controls on methane emissions from northern peatforming wetlands. *Trends in Ecology & Evolution*, *14(10)*, 385-388. https://doi.org/10.1016/S0169-5347(99)01649-3

Kayranli, B., Scholz, M., Mustafa, A. & Hedmark, Å. (2010). Carbon storage and fluxes within freshwater wetlands: a critical review. *Wetlands*, *30(1)*, 111-124.

Kidston, J., Brümmer, C., Black, T. A., Morgenstern, K., Nesic, Z., McCaughey, J. H. & Barr, A. G. (2010). Energy balance closure using eddy covariance above two different land surfaces and implications for CO_2 flux measurements. *Boundary-Layer Meteorology*, *136*, 193-218.

Knox, S. H., Sturtevant, C., Matthes, J. H., Koteen, L., Verfaillie, J. & Baldocchi, D. (2015). Agricultural peatland restoration: effects of land-use change on greenhouse gas (CO_2 and CH_4) fluxes in the Sacramento-San Joaquin Delta. *Global Change Biology*, *21(2)*, 750-765. https://doi.org/10.1111/gcb.12745

Lafleur, P. M. (2009). Connecting atmosphere and wetland: trace gas exchange. *Geography Compass*, *3(2)*, 560-585. https://doi.org/10.1111/j.1749-8198.2008.00212.x

Long, K. D., Flanagan, L. B. & Cai, T. (2010). Diurnal and seasonal variation in methane emissions in a northern Canadian peatland measured by eddy covariance. *Global Change Biology*, *16(9)*, 2420-2435. https://doi.org/10.1111/j.1365-2486.2009.02083.x

Lund, M., Lafleur, P. M., Roulet, N. T., Lindroth, A., Christensen, T. R., Aurela, M. & Nilsson, M. B. (2010). Variability in exchange of CO_2 across 12 northern peatland and tundra sites. *Global Change Biology*, *16(9)*, 2436-2448. https://doi.org/10.1111/j.1365-2486.2009.02104.x

Nahlik, A. M. & Fennessy, M. (2016). Carbon storage in US wetlands. *Nature Communications*, *7(1)*, 1-9.

Naqvi, S. M. K. & Sejian, V. (2011). Global climate change: role of livestock. *Asian Journal of Agricultural Sciences*, *3(1)*, 19-25.

Native Plant Solutions (2021). Frank Lake: Literature review and identification of potential mitigation options. Submitted to Ducks Unlimited, Edmonton, AB, Canada, April 2021. This report is publicly available via email request sent to: du_edmonton@ducks.ca

Neubauer, S. C. & Megonigal, J. P. (2015). Moving beyond global warming potentials to quantify the climatic role of ecosystems. *Ecosystems*, *18(6)*, 1000-1013.

Nisbet, R. E. R., Fisher, R., Nimmo, R. H., Bendall, D. S., Crill, P. M., Gallego-Sala, A. V. & Nisbet, E. G. (2009). Emission of methane from plants. *Proceedings of the Royal Society B: Biological Sciences, 276(1660)*, 1347-1354. https://doi.org/10.1098/rspb.2008.1731

Olsson, L., Ye, S., Yu, X., Wei, M., Krauss, K. W. & Brix, H. (2015). Factors influencing CO_2 and CH_4 emissions from coastal wetlands in the Liaohe Delta, Northeast China. *Biogeosciences*, *12(16)*, 4965-4977. https://doi.org/10.5194/bg-12-4965-2015

Petrescu, A. M. R., Lohila, A., Tuovinen, J. P., Baldocchi, D., Desai, A. R., Roulet, N. T. & Cescatti, A. (2015). The uncertain climate footprint of wetlands under human pressure. *Proceedings of the National Academy of Sciences*, *112(15)*, 4594-4599.

Randerson, J. T., Field, C. B., Fung, I. Y. & Tans, P. P. (1999). Increases in early season ecosystem uptake explain recent changes in the seasonal cycle of atmospheric CO_2 at high northern latitudes. *Geophysical research letters*, *26(17)*, 2765-2768. https://doi.org/10.1029/1999GL900500

Rinne, J., Riutta, T., Pihlatie, M., Aurela, M., Haapanala, S., Tuovinen, J. P. & Vesala, T. (2007). Annual cycle of methane emission from a boreal fen measured by the eddy covariance technique. *Tellus B: Chemical and Physical Meteorology*, *59(3)*, 449-457. https://doi.org/10.1111/j.1600-0889.2007.00261.x

Rosentreter, J. A., Borges, A. V., Deemer, B. R., Holgerson, M. A., Liu, S., Song, C. & Eyre, B. D. (2021). Half of global methane emissions come from highly variable aquatic ecosystem sources. *Nature Geoscience*, *14(4)*, 225-230.

Roslev, P. & King, G. M. (1996). Regulation of methane oxidation in a freshwater wetland by water table changes and anoxia. *FEMS Microbiology Ecology*, *19*(2), 105-115. https://doi.org/10.1111/j.1574-6941.1996.tb00203.x

Sadler, T. C., Wallis, C. & Wershler, C. (1995). Frank Lake - it's more than ducks. *Blue Jay*, *53*, 134-139. https://bluejayjournal.ca/index.php/bluejay/article/view/5460/5449

Segers, R. (1998). Methane production and methane consumption: a review of processes underlying wetland methane fluxes. *Biogeochemistry*, *41(1)*, 23-51.

Sinthumule, N. I. (2021). An analysis of communities' attitudes towards wetlands and implications for sustainability. *Global Ecology and Conservation*, *27*, e01604. https://doi.org/10.1016/j.gecco.2021.e01604

Sorrell, B. K. & Brix, H. (2013). Gas transport and exchange through wetland plant aerenchyma. *Methods in Biogeochemistry of Wetlands*, *10*, 177-196. https://doi.org/10.2136/sssabookser10.c11

Strachan, I. B., Nugent, K. A., Crombie, S. & Bonneville, M. C. (2015). Carbon dioxide and methane exchange at a cool-temperate freshwater marsh. *Environmental Research Letters*, *10(6)*, 065006. https://doi.org/10.1088/1748-9326/10/6/065006

Tangen, B. A. & Bansal, S. (2020). Soil organic carbon stocks and sequestration rates of inland, freshwater wetlands: Sources of variability and uncertainty. *Science of the Total Environment*, *749*, 141444. https://doi.org/10.1016/j.scitotenv.2020.141444

Villa, J. A., Ju, Y., Stephen, T., Rey-Sanchez, C., Wrighton, K. C. & Bohrer, G. (2020). Plant-mediated methane transport in emergent and floating-leaved species of a temperate freshwater mineral-soil wetland. *Limnology and Oceanography*, *65(7)*, 1635-1650. https://doi.org/10.1002/lno.11467

Walter, B. P. & Heimann, M. (2000). A process-based, climate-sensitive model to derive methane emissions from natural wetlands: Application to five wetland sites, sensitivity to model parameters, and climate. *Global Biogeochemical Cycles*, *14(3)*, 745-765. https://doi.org/10.1029/1999GB001204

Wang, Q., Adiku, S., Tenhunen, J. & Granier, A. (2005). On the relationship of NDVI with leaf area index in a deciduous forest site. *Remote Sensing of Environment*, *94(2)*, 244-255. https://doi.org/10.1016/j.rse.2004.10.006

Were, D., Kansiime, F., Fetahi, T., Cooper, A. & Jjuuko, C. (2019). Carbon sequestration by wetlands: a critical review of enhancement measures for climate change mitigation. *Earth Systems and Environment*, *3(2)*, 327-340.

Whalen, S. C. (2005). Biogeochemistry of methane exchange between natural wetlands and the atmosphere. *Environmental Engineering Science*, *22(1)*, 73-94. https://doi.org/10.1089/ees.2005.22.73

White, J. S. & Bayley, S. E. (1999). Restoration of a Canadian prairie wetland with agricultural and municipal wastewater. *Environmental Management*, *24(1)*, 25-37.

White, J. S. & Bayley, S. E. (2001). Nutrient retention in a northern prairie marsh (Frank Lake, Alberta) receiving municipal and agro-industrial wastewater. *Water, Air, and Soil Pollution*, *126(1)*, 63-81.

Whiting, G. J. & Chanton, J. P. (1996). Control of the diurnal pattern of methane emission from emergent aquatic macrophytes by gas transport mechanisms. *Aquatic Botany*, *54(2-3)*, 237-253. https://doi.org/10.1016/0304-3770(96)01048-0

Whiting, G. J. & Chanton, J. P. (2001). Greenhouse carbon balance of wetlands: methane emission versus carbon sequestration. *Tellus B*, *53(5)*, 521-528. https://doi.org/10.1034/j.1600-0889.2001.530501.x

Wilson, K., Goldstein, A., Falge, E., Aubinet, M., Baldocchi, D., Berbigier, P. & Verma, S. (2002). Energy balance closure at FLUXNET sites. *Agricultural and Forest Meteorology*, *113(1-4)*, 223-243.

Zhu, D., Ryan, M. C. & Gao, H. (2019). The role of water and mass balances in treatment assessment of a flooded natural wetland receiving wastewater effluent (Frank Lake, Alberta, Canada). *Ecological Engineering*, *137*, 34-45. https://doi.org/10.1016/j.ecoleng.2019.01.010

APPENDIX 1

Locations of above-ground biomass collection for LAI calculations

Location	Coordinates
N	50°31'26" N, 113◦41'07" W
E	50◦31'23" N, 113◦41'00" W
W	50◦31'22" N, 113◦41'13" W
S	50◦31'18" N, 113◦41'06" W
1	50◦31'25" N, 113◦41'07" W
2	50◦31'24" N, 113◦41'10" W
3	50◦31'20" N, 113◦41'07" W
4	50◦31'20" N, 113◦41'09" W